Reading ADP-ribosylation signaling using chemical biology and interaction proteomics

Kliza, K.W.; Liu, Q.; Roosenboom, L.W.M.; Jansen, P.W.T.C.; Filippov, D.V.; Vermeulen, M.

Molecular Cell

Resource

Reading ADP-ribosylation signaling using chemical biology and interaction proteomics

Graphical abstract

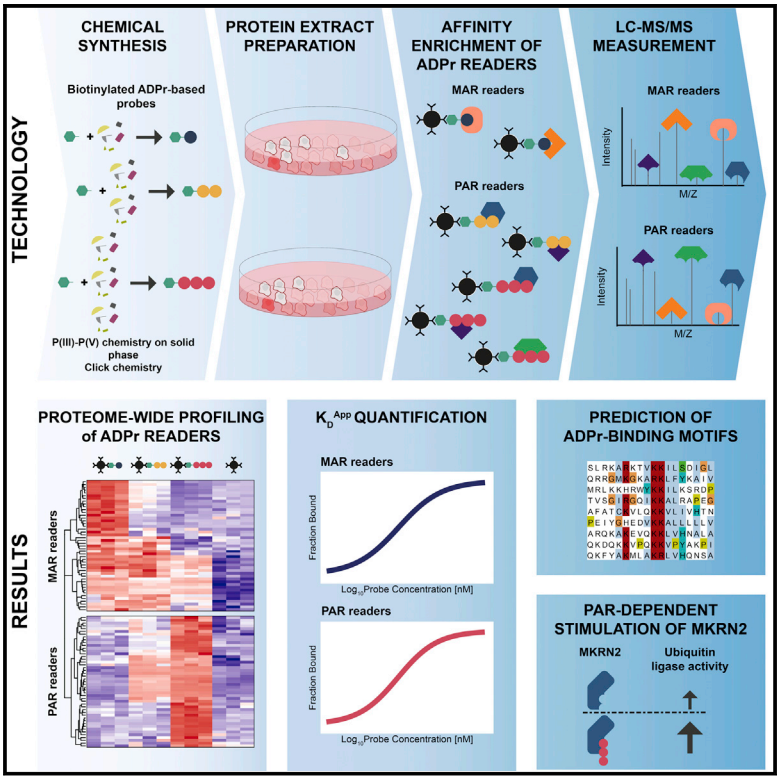

Authors

Katarzyna W. Kliza, Qiang Liu, Laura W.M. Roosenboom, Pascal W.T.C. Jansen, Dmitri V. Filippov, Michiel Vermeulen

Correspondence

k.kliza@science.ru.nl (K.W.K.), filippov@lic.leidenuniv.nl (D.V.F.), michiel.vermeulen@science.ru.nl (M.V.)

In brief

Kliza et al. synthesized biotinylated ADPr probes and used them as affinity-purification reagents to identify proteome-wide MAR and PAR readers. They also determined apparent binding affinities for ADPr readers and predicted and determined their ADPr-binding motifs. Finally, they uncovered mechanistic crosstalk between ubiquitin and ADP-ribosylation signaling.

Highlights

- Chemical biology enables proteome-wide ADPr interaction screenings
- MAR and PAR recruit distinct sets of readers
- Apparent binding affinities quantified for dozens of MAR and PAR readers
- The ubiquitin ligase activity of MKRN2 is stimulated by PAR

Kliza et al., 2021, Molecular Cell *81*, 4552–4567
November 4, 2021
https://doi.org/10.1016/j.molcel.2021.08.037

CellPress

CellPress

Molecular Cell

Resource

Reading ADP-ribosylation signaling using chemical biology and interaction proteomics

Katarzyna W. Kliza,[1,3,*] Qiang Liu,[2,3] Laura W.M. Roosenboom,[1] Pascal W.T.C. Jansen,[1] Dmitri V. Filippov,[2,*] and Michiel Vermeulen[1,4,*]

[1]Department of Molecular Biology, Faculty of Science, Radboud Institute for Molecular Life Sciences (RIMLS), Oncode Institute, Radboud University Nijmegen, 6525 GA Nijmegen, the Netherlands

[2]Leiden Institute of Chemistry, Leiden University, 2333 CC Leiden, Netherlands

[3]These authors contributed equally

[4]Lead contact

*Correspondence: k.kliza@science.ru.nl (K.W.K.), filippov@lic.leidenuniv.nl (D.V.F.), michiel.vermeulen@science.ru.nl (M.V.)

https://doi.org/10.1016/j.molcel.2021.08.037

SUMMARY

ADP-ribose (ADPr) readers are essential components of ADP-ribosylation signaling, which regulates genome maintenance and immunity. The identification and discrimination between monoADPr (MAR) and polyADPr (PAR) readers is difficult because of a lack of suitable affinity-enrichment reagents. We synthesized well-defined ADPr probes and used these for affinity purifications combined with relative and absolute quantitative mass spectrometry to generate proteome-wide MAR and PAR interactomes, including determination of apparent binding affinities. Among the main findings, MAR and PAR readers regulate various common and distinct processes, such as the DNA-damage response, cellular metabolism, RNA trafficking, and transcription. We monitored the dynamics of PAR interactions upon induction of oxidative DNA damage and uncovered the mechanistic connections between ubiquitin signaling and ADP-ribosylation. Taken together, chemical biology enables exploration of MAR and PAR readers using interaction proteomics. Furthermore, the generated MAR and PAR interaction maps significantly expand our current understanding of ADPr signaling.

INTRODUCTION

Post-translational modifications (PTMs) are essential for cellular homeostasis (Conibear, 2020). ADP-ribosylation is an abundant PTM that is catalyzed by mono-ADP-ribosyltransferases (MARTs) and polyADPr polymerases (PARPs), which transfer ADP-ribosyl (ADPr) residues from nicotinamide-adenine-dinucleotide-positive (NAD^+) to specific nucleophilic amino acid side chains (Lin, 2007; Crawford et al., 2018; Lüscher et al., 2018). ADP-ribosylation has a crucial role in processes related to genome maintenance and immunity (Gibson and Kraus, 2012; Ryu et al., 2015; Gupte et al., 2017; Fehr et al., 2018; Grunewald et al., 2019). The discovery that certain cancer types that are characterized by defective homologous recombination depend on PARP1 activity has triggered an increased interest in polyADP-ribosylation (PARylation) and resulted in the development of clinically approved PARP inhibitors (i.e., olaparib) (Ray Chaudhuri and Nussenzweig, 2017; Rimar et al., 2017; Minchom et al., 2018; Golan et al., 2019). Other components of the ADPr system are also emerging as potential drug targets (Teloni and Altmeyer, 2016; Palazzo et al., 2019; Patel et al., 2020). Despite these breakthroughs, ADP-ribosylation is still relatively poorly understood in terms of structural molecular details and regarding the proteins involved in its turnover and recognition. These shortcomings can be explained by the properties of ADPr modifications, such as the labile linkages with target proteins, the complex polyanionic structure and its dynamic nature (Kistemaker et al., 2015; Lambrecht et al., 2015). However, given its pivotal role in cellular signaling and a variety of diseases, comprehensive identification of the ADPr signaling network is of great importance.

Recent advances have provided insights into the ADP-ribosylome and enabled proteome-wide identification of ADPr acceptor proteins (Karlberg et al., 2013; Martello et al., 2016; Bonfiglio et al., 2017; Larsen et al., 2018; Hendriks et al., 2019; Kalesh et al., 2019; Buch-Larsen et al., 2020). Proteins comprising modules that bind to monoADP-ribosylated (MARylated) and PARylated targets, so-called MAR and PAR "readers," are important components of the ADPr signaling network (Teloni and Altmeyer, 2016; Kamaletdinova et al., 2019). Hitherto, one MAR- and less than a dozen PAR-binding modules have been identified (Lüscher et al., 2018). Initial efforts to identify proteome-wide ADPr readers made use of two-dimensional proteins gels and incubation of polyvinylidene fluoride (PVDF) membranes with ^{32}P-labeled PAR chains followed by MALDI-based identification of protein spots (Gagné et al., 2008). Despite these efforts, a proteome-wide map of MAR and PAR readers has not yet been reported. Chemical synthesis of

oligoADPr-containing probes represents a unique challenge (Liu et al., 2019). During the past decade, we have made significant progress toward the synthesis of well-defined fragments of ADP-ribosylated proteins and analogs thereof (van der Heden et al., 2010; Kistemaker et al., 2016; Liu et al., 2018; Voorneveld et al., 2018). We also developed efficient procedures to synthesize pyrophosphates and analogs, culminating in the assembly of short oligoADPr chains and in a methodology to acquire pyrophosphate isosteres.

Here, we applied a state-of-the-art chemical approach to synthesize biotinylated mono-, di-, and triADPr probes and used them for affinity purifications in crude mammalian cell lysates combined with quantitative mass spectrometry (MS) to generate proteome-wide ADPr interactomes. This workflow enabled the identification of numerous known and novel MAR and PAR readers, as well as cell-type-dependent and -independent PAR readers. As expected, the datasets obtained were enriched for proteins that regulate the DNA-damage response (DDR). Our results also uncovered a large number of ADPr readers that regulate other processes, such as cellular metabolism, RNA trafficking, protein secretion, and transcription. We also applied an absolute interaction proteomics method to determine apparent binding affinities for dozens of MAR and PAR readers, and we predicted numerous ADPr-binding domains for readers that were identified. Furthermore, we monitored the dynamics of ADPr interactions upon induction of oxidative DNA damage in cells, which revealed DNA-damage-induced PAR readers. We also performed extensive validation for more than a dozen ADPr readers and confirmed that these proteins directly interact with MAR and PAR chains. Finally, we identified MKRN2 as a PAR-dependent E3 ubiquitin ligase. Taken together, chemical biology enables exploration of the MAR- and PAR-binding proteins using synthetic, well-defined probes. Furthermore, the proteome-wide ADPr landscapes significantly expand our understanding of the complex ADPr signaling network.

RESULTS

Identification of ADPr readers using chemical biology and interaction proteomics

Known ADPr-binding domains recognize either the terminal ADPr, the ADPr-ADPr junction, or *iso*-ADPr (Teloni and Altmeyer, 2016). We reasoned that synthetic affinity-enrichment probes that consisted of mono- or oligoADPr could be used to identify and discriminate MAR and PAR readers. We, therefore, designed and synthesized well-defined biotinylated ADPr probes of discrete length (mono-, di-, and triADPr) for affinity-purification purposes (Figure 1A; Methods S1).

We first performed solid-phase synthesis of ADPr fragments containing a terminal alkyne using a modification of our reported method based on P(III)–P(V) chemistry (Kistemaker et al., 2015). We used TentaGel N resin to facilitate the scale up and adopted fluorenylmethyl (Fm) as a temporary protecting group to exclude partial acidolysis of the *O*-glycosidic linkages of ADPr-oligomers during the deprotection step (Methods S1). The propargylated monoADPr (2a), diADPr (2b), and triADPr (2c) were conjugated to azido-PEG_3-biotin using a copper(I)-catalyzed alkyne-azide cycloaddition to obtain biotinylated mono-, di-, and triADPr (Lambrecht et al., 2015; Liu et al., 2018) (Figure 1A).

After synthesis and purification of the ADPr oligomers, we evaluated the stability of the ADPr-based probes in crude lysates by monitoring the interaction between the known PAR reader XRCC1 and biotin-oligoADPr (Figure S1A). We observed efficient enrichment of XRCC1 in the presence of ADPr hydrolase inhibitors, whereas that interaction was not observed in the presence of the recombinant phosphodiesterase ENPP1 or the PAR hydrolase PARG. Therefore, the ADPr-based affinity enrichment probes were effectively protected against ADPr hydrolases under the selected experimental conditions.

Next, we established a quantitative MS-based workflow to identify ADPr readers (Figure 1B). Crude mammalian whole-cell extracts were incubated with biotinylated ADPr probes immobilized on streptavidin-conjugated beads. As a negative control, extracts were incubated with empty streptavidin beads. After extensive washes, bound proteins were digested with trypsin, and tryptic peptides were analyzed by high-resolution, label-free quantitative MS (LFQ-MS) analyses. Raw data were analyzed using MaxQuant and Perseus (Cox and Mann, 2008; Tyanova et al., 2016). We first determined enrichment of proteins in the ADPr affinity purifications relative to the negative control (Figures 1C, S1B, and S1C). We also compared binding preferences of proteins for the different baits against each other (Figures 1D, S1D, and S1E). More than 50 and 35 proteins exhibited at least 2-fold enrichment in affinity purifications with the triADPr and diADPr probe compared with the negative control, respectively (Figures 1C and S1B; Table S1). Reassuringly, we identified well-known ADPr readers, such as XRCC1, APTX, and RNF146/Iduna (Teloni and Altmeyer, 2016). To date, only a few MAR readers have been identified (Teloni and Altmeyer, 2016; Gupte et al., 2017). Nevertheless, we identified numerous MAR interactors, including the known MAR reader MACROD1 (Figure S1C; Table S1). Of note, comparisons of proteins interacting with tri- versus monoADPr revealed that our workflow efficiently discriminated between PAR and MAR readers (Figure 1D; Table S1).

Proteome-wide profiling of ADPr interactomes

Next, significantly enriched proteins in the affinity purifications were identified by ANOVA statistics and visualized by correlation-based clustering, which revealed 119 ADPr readers displaying selective binding to a single or multiple ADPr baits (Figure 2A; Table S1). Among these, we identified 77 putative PAR readers that were specifically enriched by either one or both oligoADPr baits (cluster "PAR"; Figure 2A). The remaining 42 proteins are classified as putative MAR readers, and a subset of these also interact with the oligoADPr baits, likely through the terminal ADPr moiety in the probes (cluster "MAR"; Figure 2A). Furthermore, integration of the data obtained with that of previously published protein copy number data for HeLa cells revealed that our ADPr interaction screening was not biased toward highly abundant proteins (Figure 2B) (Nagaraj et al., 2011).

Several known ADPr readers display a binding pattern that is consistent with previous studies (Figure 2C). Moreover, our dataset further confirmed that macrodomain-containing proteins exhibit distinct binding preferences toward ADPr modifications, including the MAR reader MACROD1, the PAR-specific CHD1L,

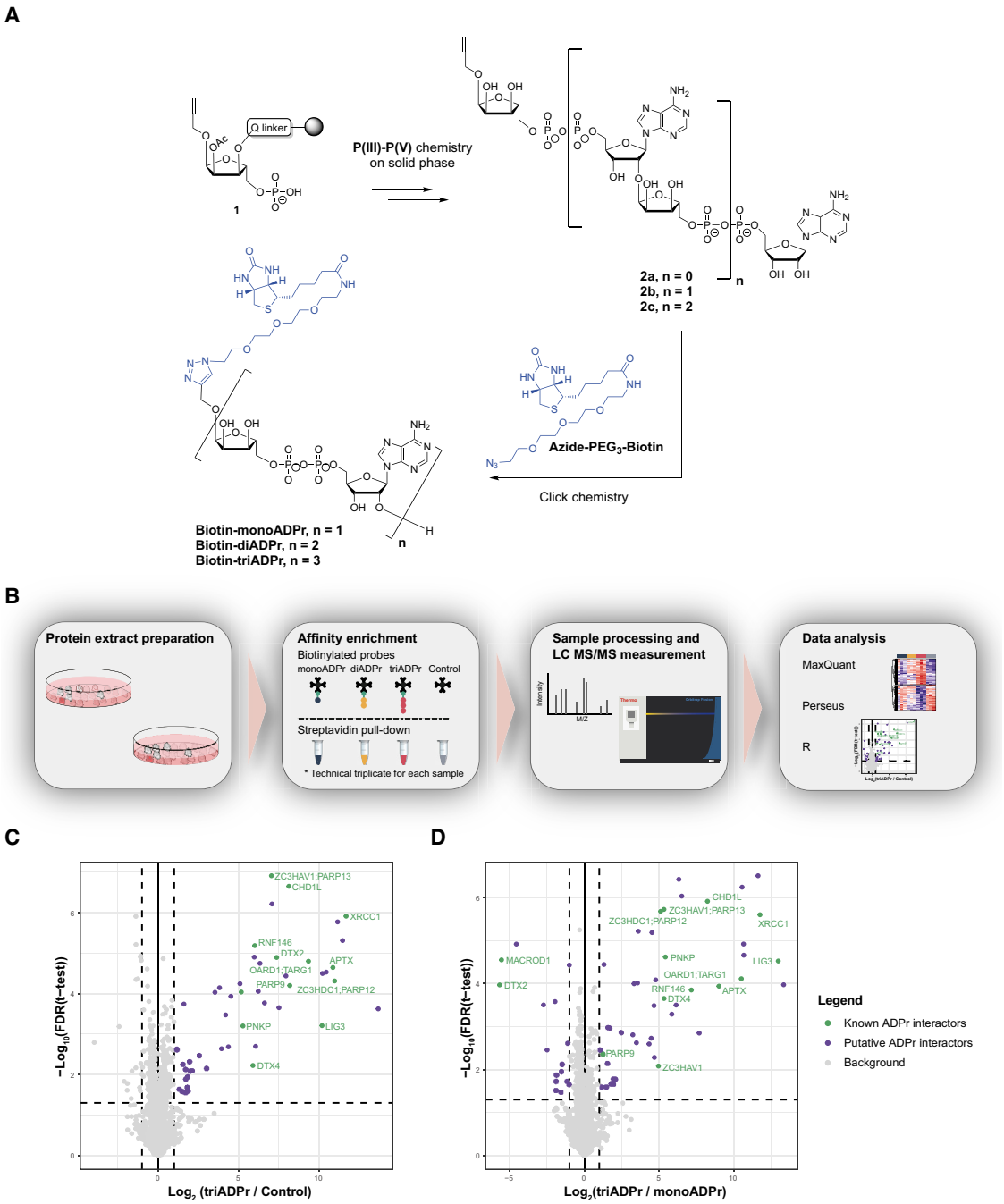

Figure 1. Synthesis of biotinylated ADPr probes for interaction proteomics

(A) Schematic overview of the synthesis of biotinylated ADPr probes.

(B) Schematic overview of the workflow of ADPr interaction proteomics.

(C and D) Volcano plots of affinity purifications of triADPr versus a negative control (C) and triADPr against monoADPr (D). Fold enrichments (FC $\geq$ 2, x axis) were plotted against $-\log_{10}$-transformed p value of the permutation-based false-discovery rate (FDR)-corrected t test (FDR < 0.05, y axis). The dashed lines represent the statistical cutoffs. A subset of known ADPr readers is labeled.

See also Figure S1 and Table S1.

and the MAR- and PAR-binding PARP9. We also uncovered numerous additional putative ADPr readers, such as the metabolic enzymes ME2, IMPDH1/2, GAPDH, ubiquitin E3 ligase MKRN2, DNA damage-sensing kinase ATR, and the receptor OGFR. Gene Ontology (GO) enrichment analyses for MAR- and PAR-specific protein clusters revealed overlapping and specific

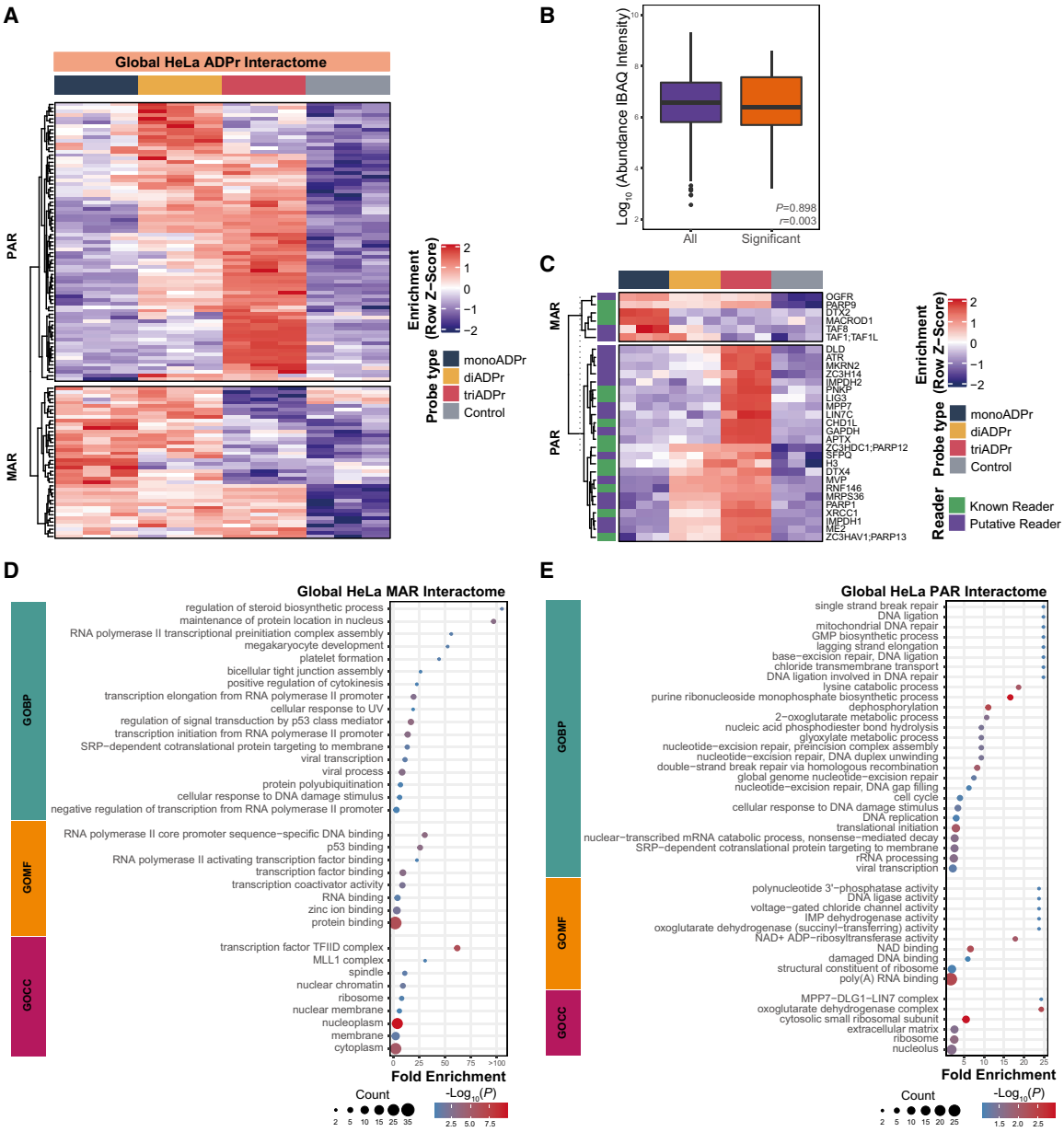

Figure 2. Global ADPr interactome in HeLa cells

(A) Hierarchical clustering of statistically significant ADPr interactors. ANOVA test thresholds are as follows: FDR = 0.03, $S_0 = 0$. Protein enrichment and lack of the enrichment are indicated in red and violet, respectively. The color coding for probe types is indicated, and the color density reflects the scale of enrichment. A cluster of proteins showing specific binding to the negative control was omitted from the heatmap.

(B) Concentration range of all HeLa proteins (All) and the amounts of significant ADPr interactors (Significant). Shown HeLa protein copy data are from Nagaraj et al. (2011). The intensity-based absolute quantification (iBAQ) algorithm for abundance intensities of all proteins and the statistically significant interactors of ADPr are presented in $\log_{10}$ scale. The data are shown as means ± SEM; the box limits indicate 25th and 75th percentiles, and the bold line represents the median value. No statistically significant difference was determined using the Mann-Whitney test (p = 0.898, r = 0.003).

(C) Heatmap showing the enrichments for identified MAR and PAR readers (top and bottom cluster, respectively). The left annotation of the heatmap indicates known and putative ADPr readers (green and violet, respectively). The color coding for the probe types is the same as in (A).

(D and E) Dot plots depicting GO term enrichment analysis for MAR (D) and PAR interactors (E). Significantly enriched GO terms ($p \leq 0.05$) are plotted against their fold enrichment. The color coding depicts $-\log_{10}(p)$ of the statistically significant terms, and dot size indicates the protein count for each term.

See also Figure S2 and Table S1.

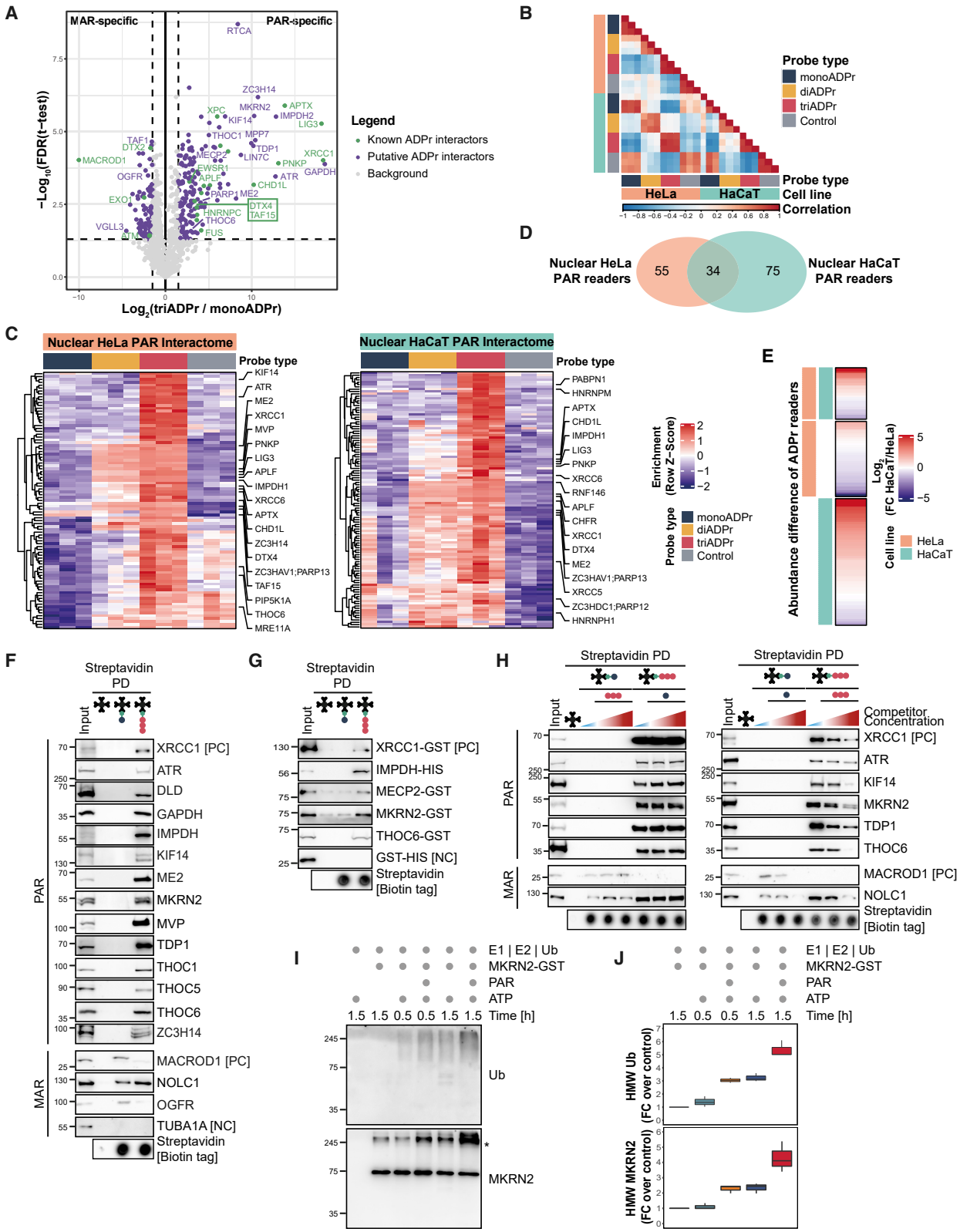

(legend on next page)

cellular functions for both ADPr modifications (Figures 2D and 2E; Table S1). As anticipated, the PAR interactome is enriched for several DNA repair pathways, including homologous recombination and nucleotide-excision repair (Gupte, Liu and Kraus, 2017). Interestingly, PAR readers are also involved in DNA processing and synthesis, diverse metabolic processes, and cell-cycle regulation. Moreover, the enrichment of terms related to RNA biology (processing and translation) is in line with previous studies (Kim et al., 2020), but our interaction screening reveals the putative PAR readers that are directly involved in these processes. In contrast, MAR readers are mainly enriched for proteins involved in regulation of transcription, cytokinesis, the cellular response to UV, tight junction assembly and metabolic processes that are distinct from those regulated by PAR readers. Furthermore, identified ADPr readers are linked to the functioning of various organs and are also associated with diseases, including cancer and viral infection (Figures S2A and S2B; Table S1).

PAR is a complex, nucleic acid-like PTM (Teloni and Altmeyer, 2016). Because of the overrepresentation of RNA biology in the gene ontology molecular function (GOMF) analysis, we further investigated the specificity of the identified ADPr interactions. Toward that aim, we profiled interactions with short nucleic acids, consisting of either three or 15 adenosine (A) compounds. This experiment revealed that oligoADPr probes and triA baits have non-overlapping interactomes and most PAR readers do not interact with longer, pentadecaA chains (Figure S2C; Table S1).

Identification of cell-type specific and constitutive PAR readers

ADP-ribosylation is an essential component of biological processes in eukaryotic nuclei (Hottiger, 2015). We, therefore, generated ADPr interactomes using nuclear extracts as input material, which resulted in the identification of 86 MAR- and 169 PAR-binding proteins (Figure 3A; Table S1), among which, were well-known PAR readers, such as FUS, XPC, EWSR1, and HNRNPC (Teloni and Altmeyer, 2016). Interestingly, a subset of proteins that were previously characterized as PAR readers, such as EXO1 and ATM, preferentially interacted with monoADPr compared with triADPr. Additional identified nuclear PAR readers include the DNA repair enzyme TDP1, the DNA methylation reader MECP2, and subunits of the THO complex.

Although basal cellular levels of PAR are low, numerous proteins have been shown to undergo PARylation (Ayyappan et al., 2021). Therefore, to ensure that identified proteins are bona fide ADPr interactors, we performed affinity purifications with nuclear extracts from cells pre-treated with the PARP inhibitor olaparib. Furthermore, the PAR network varies among different cell types (Martin et al., 2015; Zhen et al., 2017). Therefore, to identify cell-type-dependent and -independent ADPr readers, we performed additional affinity purifications with nuclear extracts from the human keratinocyte cell line HaCaT. ADPr interactomes between HeLa and HaCaT cells are correlated, indicating that many ADPr readers are constitutive and cell-type independent. TriADPr interactions, in particular, show a high degree of correlation ($p > 0.8$) (Figure 3B). This experiment resulted in the identification of 89 and 109 oligoADPr interactors with HeLa and HaCaT nuclear extracts, respectively (Figure 3C; Table S1). The interactions detected in HeLa and HaCaT cells are not strongly biased towards high-abundant proteins (Figure S3A); 34 proteins exhibited conserved binding to oligoADPr in both cell lines, whereas 55 and 75 proteins were identified as cell-type-specific PAR interactors in HeLa and HaCaT cells, respectively (Figure 3D). To determine whether cell-type-specific PAR interactions can be explained by differential protein expression, we compared protein abundances of PAR readers in HeLa and HaCaT cells (Figure 3E; Table S1). 71 PAR interactors were expressed to similar levels in both cell lines (fold change [FC] ≥ -2 and FC ≤ 2), whereas 16 proteins were not quantified (Table S1). Binding dynamics and protein abundance (FC ≥ 2, $p < 0.05$) were correlated for 31 HaCaT and 8 HeLa-specific PAR readers, respectively. Cell-type-specific, but expression-independent, binding for certain PAR readers may be explained by PTM-regulated PAR binding or cell-type-specific co-factors required for

Figure 3. Nuclear HeLa and HaCaT ADPr interactomes

(A) Volcano plot showing preferential binding of nuclear proteins to triADPr versus monoADPr. The statistical cutoffs in the t test are as follows: FC ≥ 3 and FDR < 0.05. A representative group of known and putative ADPr readers is labeled.

(B) Heatmap depicting pairwise Pearson's correlation analysis of HeLa and HaCaT nuclear ADPr interactomes.

(C) Hierarchical clustering of significantly enriched proteins by different ADPr probes in HeLa and HaCaT nuclear extracts (left and right heatmap, respectively). ANOVA test thresholds were as follows: FDR = 0.0015, $S_0 = 0$; and FDR = 0.03, $S_0 = 0$ for HeLa and HaCaT ADPr interactomes, respectively. A cluster of proteins showing specific binding to the negative control was omitted from the heatmap to ease data presentation.

(D) Venn diagram depicting the overlap between identified ADPr readers in HeLa and HaCaT nuclear extracts.

(E) Heatmap depicting the abundances of conserved, HeLa- and HaCaT-specific ADPr readers (top, middle, and bottom clusters, respectively). The statistical thresholds in t test are as follows: FC ≥ 2 and FDR < 0.05.

(F) Affinity purifications, with empty beads, mono- and triADPr baits in HeLa extracts, were subjected to immunoblotting using antibodies against proteins of interest. TUBA1A served as a negative control, whereas XRCC1 and MACROD1 were used as positive controls for PAR and MAR interactions, respectively.

(G) Validation of ADPr readers using affinity purifications with recombinant proteins. XRCC1-GST and GST-6xHIS were used as positive and negative controls, respectively.

(H) Competition-binding assays for selected ADPr interactors. Streptavidin pull-downs with empty beads, biotinylated mono- and triADPr probes were performed in HeLa extracts in the presence of increasing concentration of free probes. Left: free triADPr and untagged monoADPr were used for affinity purifications with biotinylated monoADPr and triADPr. Right: the same type of biotin-tagged and free ADPr probe was used to outcompete ADPr readers.

(I) MKRN2 *in vitro* ubiquitination assay. Top and bottom immunoblots show HMW conjugates of Ub and autoubiquitinated MKRN2, respectively.

(J) Quantification of (I). Results of independent replicates are shown as means ± SEM; the box limits represent 25th and 75th percentiles, and the bold line indicates median value.

Experiments shown in (F)–(I) were repeated independently at least three times. See also Figure S3 and Table S1.

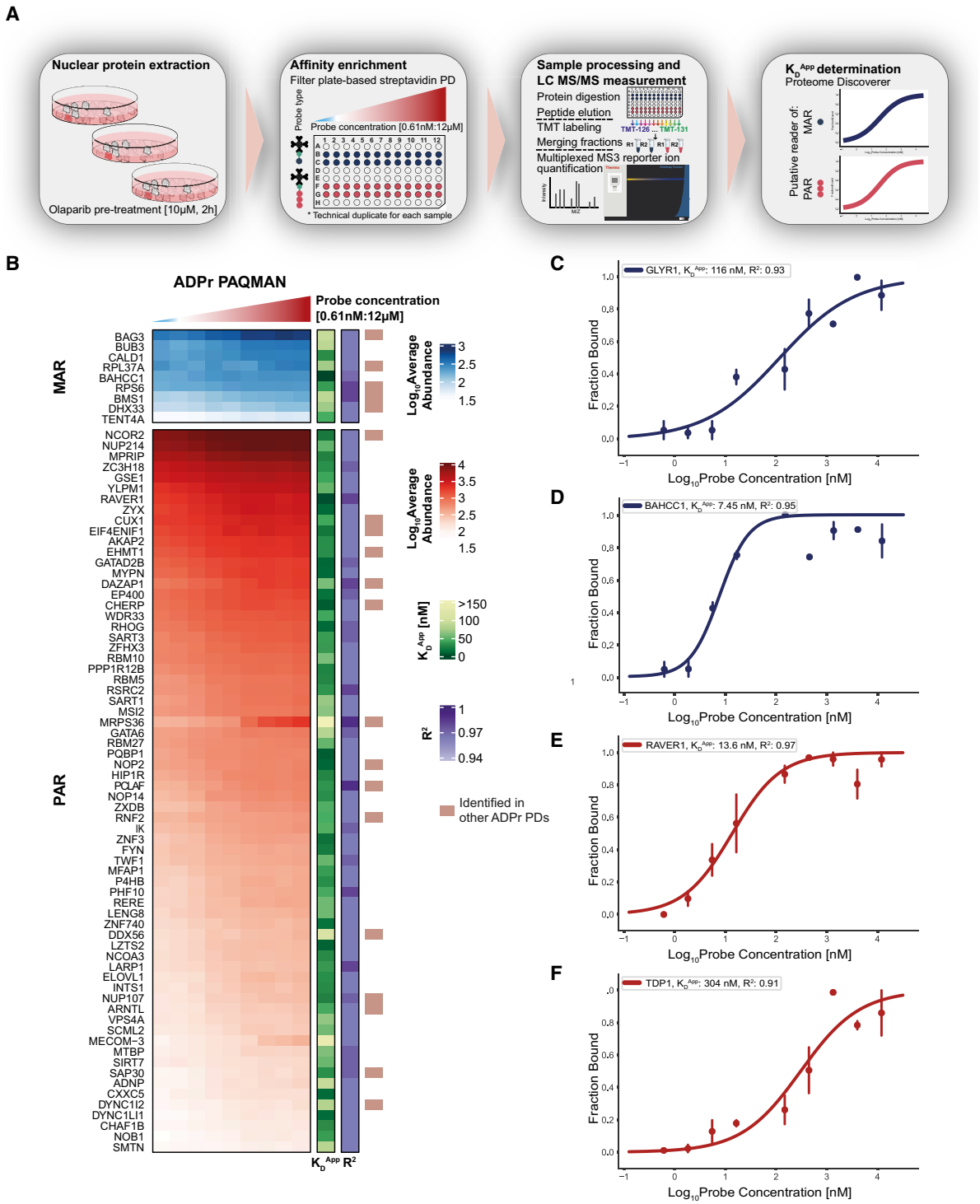

Figure 4. Quantification of apparent binding affinities between proteins and ADPr probes

(A) Schematic overview of the PAQMAN method for K_D^{App} determination for ADPr readers.

(B) Heatmaps showing PAQMAN measurements for a representative group of ADPr readers. The heatmap on the left depicts mean of grouped abundances of proteins identified in both replicates in log_{10}-scale, followed by heatmaps illustrating calculated K_D^{App} and R^2 confidence interval of the quantifications. On the

(legend continued on next page)

PAR recognition. GO term enrichment analysis revealed that conserved PAR readers are involved in the DDR and regulation of metabolic processes (Figures S3B–S3D; Table S1). Furthermore, both datasets show significant enrichment of terms related to guanosine triphosphate (GTP) biosynthesis and interferon production. Of note, the screening revealed a largely unexplored function of cell-type-independent ADPr readers in cell adhesion. HeLa-specific PAR readers are associated with DNA replication, mRNA splicing, and histone acetylation. Among overrepresented HaCaT-specific terms are melanosome and actin filament polymerization. Interestingly, mature melanosomes are transferred to keratinocytes, and one of the identified expression-dependent, HaCaT-specific PAR readers, RAB38, is implicated in melanosome trafficking (Ohbayashi and Fukuda, 2020). Furthermore, the actin cytoskeleton is an essential regulator of keratinocyte mechanosensing (Laly et al., 2021), and one of the identified PAR readers in HaCaT cells, PFN1, is indispensable for the assembly and organization of the actin cytoskeleton (Skruber et al., 2020). It is tempting to speculate that PARylation and PAR readers are involved in these processes.

Next, we verified the binding specificity for 20 identified ADPr readers using affinity purifications combined with western blotting, together with two positive controls (MACROD1 and XRCC1 for MAR and PAR, respectively). Selected proteins were validated using antibodies against endogenous proteins or by using ectopically expressed tagged proteins (Figures 3F, S3E, and S3F). These validations are in excellent agreement with the proteomics data. Furthermore, affinity purifications using recombinantly expressed proteins confirmed that, at least a subset of the identified PAR readers, MKRN2, IMPDH, THOC6, and MECP2, interact directly with ADPr chains (Figures 3G and S3G). The specificity of selected MAR and PAR readers was further verified in competition assays with free, untagged mono- and triADPr (Figure 3H).

One of the validated PAR readers, MKRN2, contains a signature RING ZF C3HC4 and exhibits E3 ligase activity (Shin et al., 2017). That protein has previously been implicated as a potential therapeutic target in melanoma (Guo and Zhang, 2020). The E3 ligase activity of RNF146/Iduna is stimulated by PAR binding (Kang et al., 2011). To investigate whether MKRN2 undergoes similar regulation, we performed an *in vitro* ubiquitination assay using recombinant MKRN2 in the absence or presence of PAR polymers. Indeed, we observed an increase in high-molecular-weight (HMW) ubiquitin conjugates and autoubiquitinated MKRN2 upon incubation of MKRN2 with ADPr chains prior to the *in vitro* ubiquitination assay (Figure 3H).

Proteome-wide quantification of apparent binding affinities of ADPr readers

Several methods have been applied to determine affinities between PAR and their readers, including electromobility shift assays, polymer-dot blot assays, isothermal titration calorimetry, and surface plasmon resonance (Krietsch et al., 2013). However, the binding affinities for the same PAR:PAR reader pair sometimes deviate by several orders of magnitude when different approaches are used (Krietsch et al., 2013). Moreover, these methods are labor intensive and low throughput. We recently developed a method called protein-nucleic-acid affinity quantification by mass spectrometry (PAQMAN), which can be used to determine apparent binding affinities for dozens of nuclear proteins and a nucleic acid sequence of interest in a single experiment (Makowski et al., 2018; Gräwe et al., 2020). Here, we have adopted the PAQMAN method to quantify apparent binding affinities between ADPr readers and MAR and PAR baits (Figure 4A). Briefly, serial dilutions of the mono- and triADPr probes in a concentration range between 0.61 nM and 12 μM were pre-bound to streptavidin-conjugated beads and incubated with a fixed amount of olaparib-pretreated HeLa nuclear extracts. Next, beads were rapidly washed, after which the affinity purification series for each bait was digested with trypsin, followed by 10-plex Tandem Mass Tag (TMT) isobaric labeling and quantitative MS analysis. The datasets were then analyzed using Proteome Discoverer and Python software. It is important to note that to determine a Hill-like curve, protein binding needs to reach saturation at the highest titration points, thus, preventing determining K_D values in the sub-millimolar range, given the bait concentration range used. To generate a high-quality list of ADPr readers and associated K_D values, we filtered out proteins that were not identified in each biological replicate. Hill-like K_D curves could be generated for 53 MAR and 208 PAR readers ($r^2 \geq 0.9$) (Figures S4A and S4B), and 65 of those proteins were identified as specific ADPr interactors in our LFQ-MS datasets (Figures 4B and S4C; Table S1). For one of identified proteins, AIFM1/AIF, the affinity for PAR was previously determined to be 66.3 nM using a polymer blot assay (Wang et al., 2011), which is in a good agreement with our PAQMAN measurement (K_D^{App} = 25.4 nM, r^2 = 0.92) (Figure 4B). In general, K_D^{App}s for quantified MAR readers are in the sub-micromolar range (Figures 4B, 4C, and S4D), whereas PAR readers exhibit K_D^{App}s in the nanomolar range (Figures 4B, 4E, and S4E). As described earlier, MAR readers are implicated in the regulation of transcription (Figure 2D). For example, GLYR1/NDF, which binds MAR with an apparent K_D^{App} value of 116 nM, facilitates RNA polymerase II transcription through nucleosome destabilization (Fei et al., 2018) (Figure 4C). BAHCC1, which was recently identified as an H3K27me3 reader that mediates gene silencing, interacts with MAR with a very high affinity (7.45 nM, r^2 = 0.95) (Figure 4D). Interestingly, BAHCC1 interacts with H3K27me3 through its BAH (bromo-adjacent homology) domain (Fan et al., 2020). Immediately adjacent to that is a putative ADPr-binding domain. It would be interesting to determine whether PAR recognition regulates H3K27me3 binding and the biological function of BAHCC1. PAR readers for which a K_D^{App} values could be determined and which have been shown to interact specifically with PAR

right, proteins identified as specific ADPr readers in the other ADPr interaction screenings are depicted. Only MAR and PAR readers with $R^2 \geq 0.94$ are shown on the top and bottom of the heatmap, respectively.
(C–F) K_D^{App} binding curves for MAR readers GLYR1 (C), BAHCC1 (D) and PAR interactors RAVER1 (E) and TDP1 (F). Each data point represents the mean of two replicates and the error bars denote the SEM.
See also Figure S4 and Table S1.

(as shown in Figures 2A, 3A, and 3C) include RAVER1 and GNAI3. RAVER1 is a ribonucleoprotein that modulates an innate antiviral response (Chen et al., 2013) (Figure 4E). GNAI3 is a GTPase, which is implicated in cell division (Cho and Kehrl, 2007) and interacts with PAR with a very high affinity (K_D^{App} 8.37 nM, r^2 = 0.93) (Figure S4E). Other proteins, such as TDP1 (Heublein et al., 2014) and MRPS36, interact with PAR with a lower affinity (K_D^{App}s 304 nM and 712 nM, respectively) (Figures 4F and S4F). For a subset of proteins, apparent K_Ds could be determined for both the mono- and triADPr probes (Figure S4G). Proteins such as PCLAF and NOL8 interact with both baits with very similar apparent K_Ds, which suggests that they recognize the terminal ADPr unit. Other proteins preferentially bind PAR, an example being the nucleolar protein NOP2, which shows a 6-fold greater affinity for PAR compared with MAR (127 nM for mono- and 20 nM for triADPr). In summary, these PAQMAN experiments verify some of the results obtained in our interaction proteomics screenings (Figures 1, 2, and 3; Table S1). As such, MAR and PAR PAQMAN experiments help guide future follow-up experiments.

Exploration of ADPr-reading motifs and their disease associations

A dozen domains have been described as ADPr interaction modules (Lüscher et al., 2018); 40 previously reported ADPr readers were covered in our ADPr interaction-proteomics screenings, and 36 of those contain a well-characterized ADPr-binding domain. (Figure 5A). *In silico,* studies predicted the PAR-binding motif (PBM) as a prevalent PAR interaction domain (Pleschke et al., 2000; Teloni and Altmeyer, 2016). Most known PAR readers that were detected in our datasets comprise a PBM domain. Moreover, we identified proteins that were previously shown to bind ADPr modifications through either macrodomain, FHA, BRCT, PBZ, PIN, OB, RING ZF of C3HC4 type, RRM, RG/RGG, SR- or KR-rich motifs (Teloni and Altmeyer, 2016). In addition, we identified four known ADPr readers with uncharacterized ADPr-binding modules. Thus, the probes used in this study allowed us to capture ADPr readers with distinct ADPr-interacting domains. Next, putative ADPr-reading motifs were identified by scanning protein sequences of MS candidates against consensus sequences of known ADPr-binding modules using ScanProsite software and further verification using the InterPro database (Figure S5A) (de Castro et al., 2006; Blum et al., 2021). This resulted in the identification of ADPr-binding modules in 212 novel ADPr readers, including 40 MAR and 172 PAR readers (Figure S5B; Table S1). Strikingly, this analysis revealed that the most prevalent ADPr-binding modules are RG/RGG-, SR-, and KR-rich motifs, followed by RRM and PBM in PAR and MAR readers, respectively. Both RG/RGG-, SR-, KR-rich motifs and RRM recognize ADPr modifications via positively charged amino acid residues, and PBM is believed to establish electrostatic interactions with PAR (Teloni and Altmeyer, 2016) (Figure 5B). However, dozens of identified MAR and PAR readers contain putative PBM motifs, suggesting the existence of MAR- and PAR-specific PBMs. Numerous ADPr readers identified in our screenings, such as THOC6, CHAF1B, PRPF4, and PRPF19, contained at least one WD40 domain, which may interact with PAR via electrostatic interactions, and has previously been described for the FBXW7 (Zhang et al., 2019). These findings provide further evidence that basic electrostatic regions exposed on protein surfaces might be the main drivers of PAR recognition. Moreover, we did not identify any MAR readers containing either an OB-fold or PBZ domain, suggesting that these reader domains are PAR specific. Numerous identified ADPr readers comprise multiple putative ADPr-reading regions (Figures 5C and S5B). E3 ligase activity of RNF146/Iduna is allosterically activated by cooperative recruitment of PAR polymers by its WWE and RING ZF domain (DaRosa et al., 2015). In our interaction proteomics screenings, we identified 11 RING ZF C3HC4-containing E3 ligases, and four of those proteins also contained putative ADPr-binding domains, such as PBM, RRM, and WD40 (Figure 5C). Hence, the RNF146/Iduna-type of activation mechanism could be a more-general phenomenon. To investigate the accuracy of the ADPr-binding domain prediction analysis, we mutated the PBM domain of the PAR reader MVP (Figure 5D). These experiments revealed that single amino acid mutants of MVP (R507A, R511A, and R512A) interact with biotin-triADPr, whereas double mutants (R507/511A, R507/512A, and R511/512A) exhibit strongly reduced binding. Finally, mutation of three amino acids in the MVP PBM domain (R507A/R511A/R512A) completely abolished triADPr binding. Next, we aimed to determine the PAR-binding regions for the readers, which lack any obvious PAR-binding domains. Thus, we generated truncation mutants of TDP1 and MKRN2 and investigated their PAR-binding ability (Figures 5E and 5F). These experiments revealed that TDP1 does not interact with PAR through its PARP1- and DNA ligase 3-interaction domains but through its catalytic domain. The recruitment of MKRN2 to PAR is mediated by its C terminus, with its C3H1 ZF domain at least partially being involved in PAR binding. The close proximity between the MKRN2 RING domain and its PAR-recognizing module provide further support for PAR-binding-mediated regulation of its E3 ligase activity.

To investigate associations between ADPr readers and diseases, we mined the Online Mendelian Inheritance in Man (OMIM) database and the DisGeNET platform (Amberger et al., 2009; Piñero et al., 2019), which annotates genes and their disease-relevant variants (Table S1). This analysis revealed that 30 MAR and more than 90 PAR readers with predicted ADPr-binding domains have been linked to various diseases, most notably cancer (Figure S5C). Moreover, mutations in a subset of ADPr readers are associated with neurodegenerative disorders (i.e., amyotrophic lateral sclerosis, spinocerebellar ataxia, and dystonia), as well as schizophrenia, microcephaly, and various types of mental retardation, which is in good agreement with previously characterized roles for ADPr signaling in cancer and neurodegeneration (Hoch and Polo, 2019). Our analysis indicates that susceptibility to cardiomyopathy, liver cirrhosis, polycystic ovary syndrome, dermatologic disorders, and HIV infections are linked to mutations in a subset of PAR readers. Interestingly, 18 identified ADPr readers harbor disease-relevant point mutations within their ADPr-binding domain (Figures S5D and S5E; Table S1). Mutations in the PBM of the MAR-binding ribosome biogenesis factor BMS1 causes the skin condition aplasia cutis congenita (Marneros, 2013), whereas a Asp154Gly mutation in the WD40

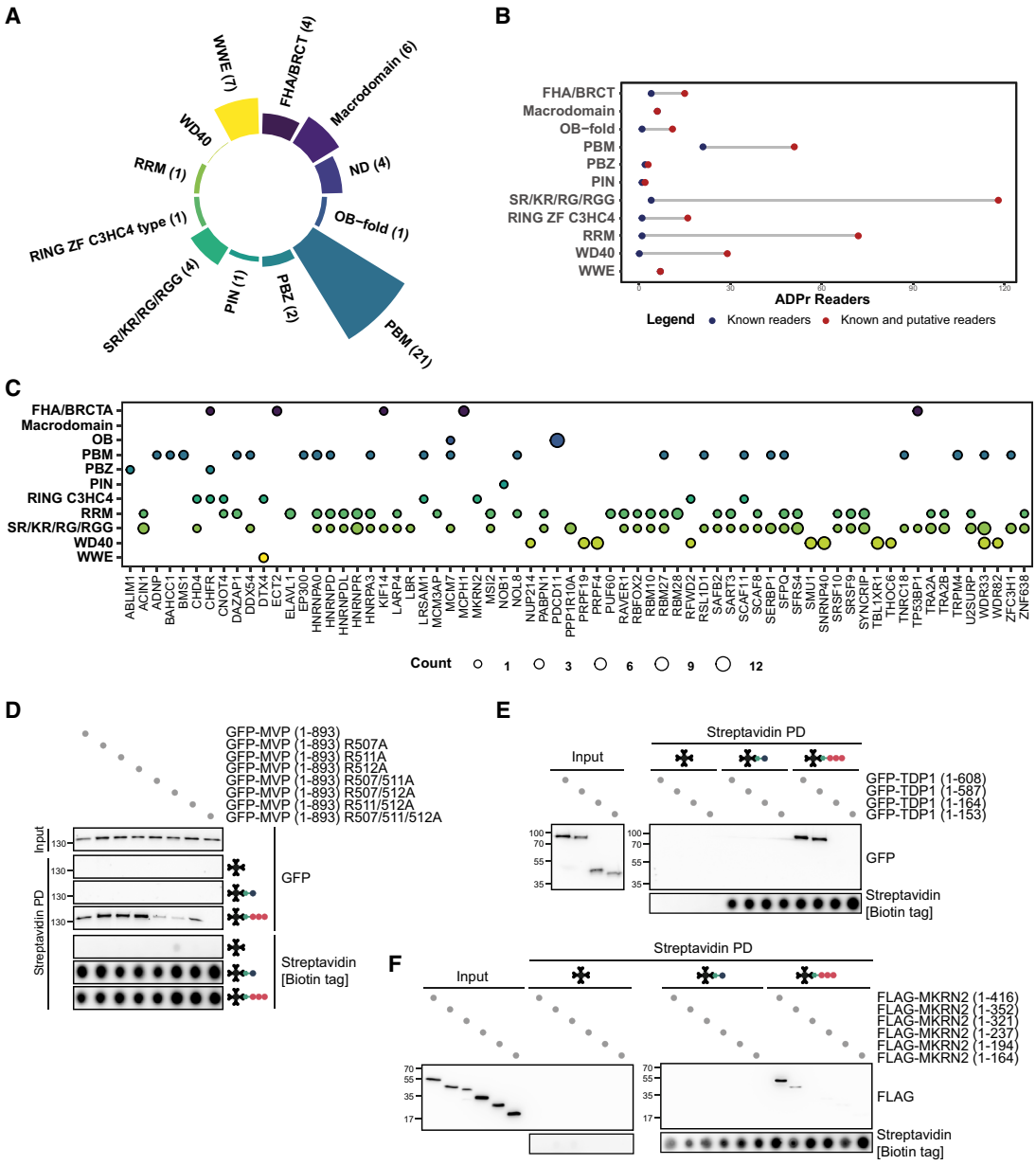

Figure 5. PAR-binding modules in ADPr readers and disease associations

(A) Circular bar plot depicting the ADPr-binding modules in previously characterized ADPr readers covered in the ADPr proteomics screenings. The number of proteins with an ADPr-interacting region is shown in brackets.

(B) Dot plot comparing the number of known ADPr readers (blue) and total number of proteins with either known or predicted ADPr-binding modules (red) found in screenings.

(C) Dot plot depicting the putative ADPr-binding modules in representative ADPr readers. The dot size denotes the domain count for each protein.

(D) ADPr affinity purifications were performed with lysates containing wild-type MVP-GFP and its single, double, and triple amino-acid PBM mutants.

(E and F) The PAR-binding potential of full-length TDP1-GFP (E) and MKRN2-FLAG (F) as well as their truncated variants was assessed by ectopic expression followed by ADPr affinity purifications.

Experiments shown in (D)–(F) were repeated independently at least two times with similar results. See also Figure S5 and Table S1.

domain of the PAR-specific nuclear pore complex subunit NUP214 results in acute encephalopathy (Shamseldin et al., 2019). Furthermore, mutations within three WD40 domains of the THOC6 subunit of the THO complex are associated with a Beaulieu-Boycott-Innes syndrome (Amos et al., 2017). Recent structural studies revealed that THOC6 is required for tetramerization of THO-UAP56 complex (Pühringer et al., 2020), and disease-relevant mutations within THOC6 disturb

its interaction with other subunits of the THO complex (Mattioli et al., 2019). It is, therefore, tempting to speculate that PAR-recognition by THOC6 modulates assembly of the THO complex under stress conditions.

Mapping dynamic ADPr interactions under oxidative stress conditions

Next, we evaluated the suitability of the ADPr probes to identify dynamic ADPr interactions under stress conditions. Toward that aim, we treated HeLa cells with hydrogen peroxide, an insult known to induce a PAR-dependent DDR (Palazzo et al., 2018). Cells were harvested at 0, 5, and 30 min after treatment, at which point a marker for cellular DNA damage, γ-H2AX, was strongly induced (Figure S6A). Most of the immediate hydrogen-peroxide-induced responses occur on chromatin, we, therefore, used chromatin-enriched nuclear extracts as the input for ADPr affinity enrichments. Correlation-based clustering revealed 355 ADPr interactors exhibiting distinct probe-binding specificity and interaction dynamics (Jungmichel et al., 2013) (Figure S6B; Table S1). This analysis resulted in the identification of 10 and 22 proteins that interact with MAR in a stimulus-independent and -dependent manner, respectively. Furthermore, 80 constitutive PAR readers were identified, including well-characterized APTX, DNA ligase 3, and XRCC1; 243 PAR readers displayed hydrogen-peroxide-dependent binding kinetics. Several of them most prominently interacted with the triADPr probe early after induction of DNA damage (clusters 4 and 8), whereas other proteins peaked 30 min after induction of DNA damage (cluster 5). ADPr binding for another group of proteins (cluster 6) was inhibited upon the treatment. Reassuringly, four clusters of dynamic DNA-damage-dependent PAR interactors are rich in DDR factors (Figure 6A). Some of these proteins were previously shown to be recruited to DNA damage foci in a PAR-dependent manner, such as KDM4D (Khoury-Haddad et al., 2014, 2015). In the future, it will be of interest to identify the mechanisms responsible for regulating dynamic, stimulus-dependent interactions between ADPr modifications and their readers. Some of these underlying mechanisms may include PTM-dependent regulation of ADPr binding affinity.

Finally, we integrated the generated DNA damage-regulated ADPr interactome with a genome-wide DNA damage CRISPR screen (Olivieri et al., 2020). This screen identified ~1,000 genes whose loss resulted in resistance or sensitivity to various DNA damage insults. 25 CRISPR-Cas9 dropout screens were performed in human RPE-1- hTERT cells. In each screen, two conditions were compared: an untreated group (control), and cells exposed to sublethal doses of drugs for 10 cell-doubling times. The drug selection enabled coverage of a wide range of DNA repair pathways in the screen. 277 proteins were common in both datasets (Figure 6B; Table S1). For example, depletion of ADPr readers SNRNP40, MYH9, PPP1R8, and SRSF10 is lethal under DNA replicative stress induced by either gemcitabine or Cdc437. Furthermore, deficiency of SRSF9, SRSF6, BAZ1B, and several other putative PAR readers causes cellular sensitivity toward DNA strand-breaking-inducing agents bleomycin and camptothecin. Strikingly, depletion of a plethora of dynamic ADPr readers is associated with cellular resistance to duocarmycin, calicheamicin, and trabectedin. Duocarmycin and calicheamicin are antitumor antibody-drug conjugates exhibiting high cytotoxicity, whereas trabectedin is an isoquinoline alkylating agent used for chemotherapy (Pignochino et al., 2017). Interestingly, PARP inhibitors were shown to augment antitumor and antimetastatic activity of trabectedin in mice. Noteworthy, genotoxic sensitivity to these three agents is reduced by depletion of 16 identified ADPr readers, including the RNA helicases DDX54 and DDX56. These proteins might represent a class of ADPr readers whose expression is required for effective anti-cancer therapy with duocarmycin, calicheamicin, or trabectedin. In summary, these integrative analyses further confirm and expand the intricate connection between ADP-ribosylation, the DDR and cancer therapy.

DISCUSSION

In this study, we have combined chemical synthesis of structurally defined biotinylated ADPr probes with interaction proteomics technology to identify hundreds of putative MAR and PAR readers (Figures 1, 2, 3, 4, 6, and 7A). These experiments revealed that certain domains, which were previously considered to be exclusively PAR specific, also interact with MAR, such as the PBM. Furthermore, certain proteins, which were previously described as PAR readers, such as EXO1, DTX2, and ATM, actually also interact with MAR. Future structural studies are required to reveal the underlying molecular mechanisms.

When we were preparing this manuscript, two proteomics approaches to identify PAR readers were reported. Lam et al. (2021) synthesized a bifunctional NAD^+ probe with C2-diazirine and clickable ribose, which serves as a PARP1 substrate, thus, enabling identification of PARylation-dependent interactors. Dasovich et al. (2021) generated a biotinylated, photoaffinity-based PAR probe, which enabled the identification of a large number of direct PAR readers. 26 PAR readers were identified in all three studies, including ours (Figure 7B). A significant overlap of 72 and 184 proteins was found between our study and the datasets of Lam et al. (2021) and Dasovich et al. (2021), respectively. A quantitative comparison between MAR and PAR readers, however, is currently only possible using the toolkit presented in this study.

Our proteomics screenings significantly expand on previously described functional connections between ubiquitin signaling and ADP-ribosylation. In particular, we identified a number of E3 ligase proteins as ADPr readers. We demonstrated that the E3 ligase activity of MKRN2 is stimulated by the addition of PAR chains *in vitro*. The fact that the interaction between PAR and MKRN2 is mediated by its zinc finger (ZF)-comprising C terminus suggests PAR-binding-induced allosteric activation of its RING active site. In the future, it will be interesting to determine whether PAR-dependent regulation of the MKRN2 ubiquitin ligase activity is functionally connected to its previously described physiological and pathological role in cancer and inflammation. In a more-general sense, many identified ADPr readers have previously been implicated in various diseases (McGurk et al., 2019; Palazzo et al., 2019). In the future, these connections could be further investigated, and eventually, targeting certain ADPr-reader interactions may turn out to be beneficial from a therapeutic perspective.

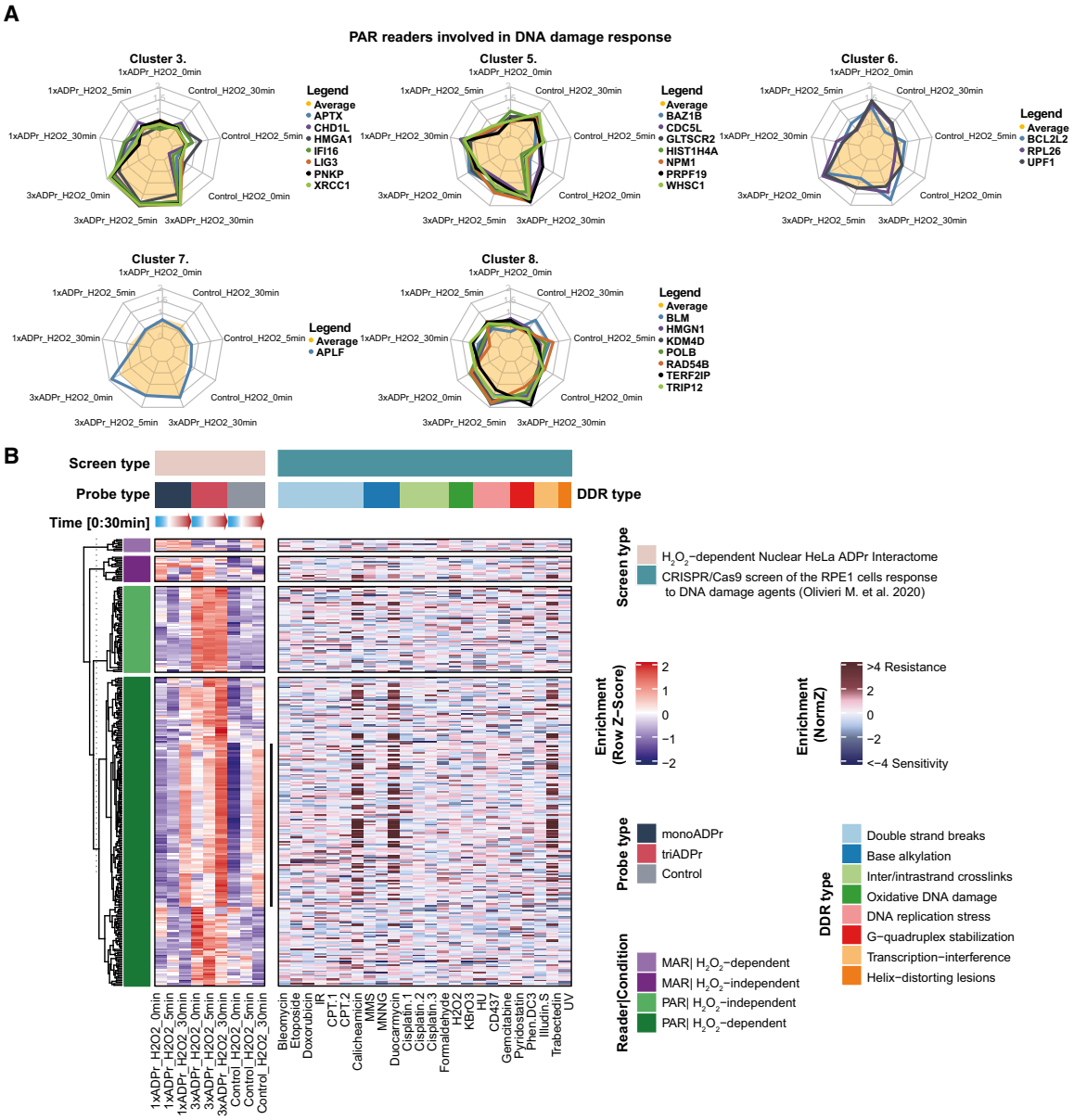

Figure 6. DNA damage-dependent ADPr readers and data integration with a genome-wide DDR CRISPR screening

(A) Radar charts showing enrichment of k-means-clustered ADPr interactors with or without H_2O_2 treatment at different time points. The yellow area depicts the mean enrichment of the ADPr readers within the cluster. Additionally, the binding dynamics for a subset of known DNA damage proteins is shown. The distance from the canter to periphery indicates protein enrichment for each probe at different time points after H_2O_2 treatment. The heatmap for k-means clustering is shown in Figure S6B.

(B) Heatmaps comparing H_2O_2-dependent ADPr interactors (this study) with a published genome-wide CRISPR screen of the DDR. Proteins common to both screenings are shown. The left heatmap depicts a subset of ADPr interactors at different time points after H_2O_2 treatment (2 mM) (Figure S6B). A subset of proteins in the bottom cluster also displays a stimulus-dependent increase in the negative control (indicated with a black line). The right heatmap represents the survival of cells depleted for those ADPr readers upon exposure to diverse DNA-damaging agents.

See also Figure S6 and Table S1.

Limitations of the study

The synthesized ADPr baits represent first-generation probes, which lack functional groups for photo-crosslinking to enable mapping-direct ADPr readers, as recently shown by Dasovich et al. (2021). The proteins identified in our screenings, thus, represent a mixture of direct and indirect ADPr readers. However, around one-third of all the identified proteins carry a putative ADPr-binding domain, suggesting that many of them interact with ADPr directly. Furthermore, we validated a number of direct ADPr readers using recombinant proteins. Thus far, a few

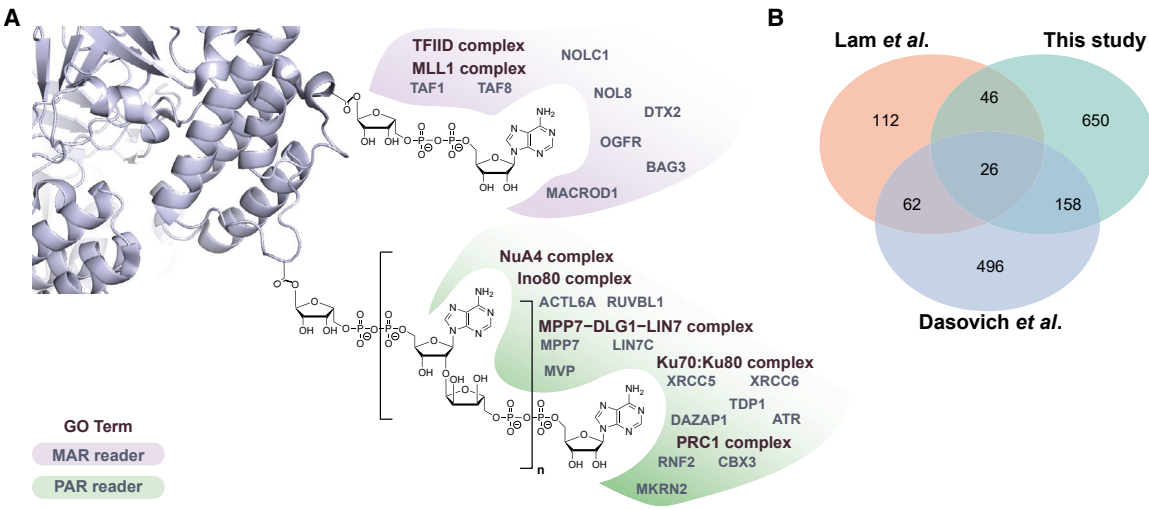

Figure 7. An interaction landscape of ADPr signaling

(A) Schematic overview of a subset of discovered MAR and PAR readers and selected protein complexes, whose subunits were identified as ADPr readers.
(B) Venn diagram depicting the overlap of identified ADPr readers between this study, the Lam et al. (2021) study, and the Dasovich et al (2021) study.
See also Table S1.

proteins were shown to specifically interact with very long PAR chains, such as DEK and XPA (Fahrer et al., 2007, 2010). The identification of such PAR readers would require much-longer probes compared with those we used. Furthermore, current probes are not suitable for identifying readers that interact with branched PAR chains. Finally, certain proteins may require conjugation of MAR and PAR to a peptide backbone to generate a high-affinity binding site.

STAR★METHODS

Detailed methods are provided in the online version of this paper and include the following:

- KEY RESOURCES TABLE
- RESOURCE AVAILABILITY
  - Lead contact
  - Materials availability
  - Data and code availability
- EXPERIMENTAL MODEL AND SUBJECT DETAILS
  - Cell culture
- METHOD DETAILS
  - Drug treatment
  - Plasmid constructs
  - Plasmid DNA transfection
  - Protein extract preparation
  - ADPr affinity purifications
  - ADPr competition binding assay
  - ADPr PAQMAN experiments
  - On-bead digestion
  - Chemical synthesis of biotinylated oligoADPr probes
  - ADPr affinity purification with recombinant proteins
  - *In vitro* ubiquitination assay
  - Immunoblotting
  - Proteome analysis
  - Mass spectrometry
- QUANTIFICATION AND STATISTICAL ANALYSIS
  - General information
  - Mass spectrometry data analysis

SUPPLEMENTAL INFORMATION

Supplemental information can be found online at https://doi.org/10.1016/j.molcel.2021.08.037.

ACKNOWLEDGMENTS

We thank Pablo Radicella (Francois Jacob Institute of Biology), Teruko Tamura-Niemann (Medizinische Hochschule Hannover), Cheng-Lung Hsu (Chang Gung University), Fritz Boege (Universitatsklinikum Dusseldorf), Erik A.C. Wiemer (Erasmus MC), Hideki Yamaguchi (Sasaki Institute), Scott B. Vande Pol (University of Virginia), and Takashi Tanaka (RIKEN Center) for providing reagents. We thank the Vermeulen and Filippov laboratories for fruitful discussions. We thank Cathrin Gräwe and Velin M. Sequeira for help with the PAQMAN experiments, and we thank Nico J. Meeuwenoord for technical assistance. The Vermeulen laboratory is part of the Oncode Institute, which is partly funded by the Dutch Cancer Society. This research was supported by an NWO-CW-TOP grant (TOP.017.010). K.W.K. is supported by EMBO long-term fellowship ALTF 847-2019, and Q.L. is supported by the Chinese Scholarship Council (CSC).

AUTHOR CONTRIBUTIONS

K.W.K., D.V.F., and M.V. conceived the project. Q.L. designed and synthesized ADPr affinity enrichment probes. K.W.K. and L.W.M.R. performed most of the proteomics and biochemical experiments. P.W.T.C.J. performed the filter-aided sample preparation (FASP) analysis and measured the MS samples. K.W.K. analyzed the MS data and made related figures. K.W.K. and M.V. wrote the paper with input from D.V.F. and Q.L. M.V. and D.V.F. supervised the project.

DECLARATION OF INTERESTS

The authors declare no competing interests.

Received: February 19, 2021
Revised: July 23, 2021
Accepted: August 26, 2021
Published: September 21, 2021

SUPPORTING CITATIONS

The following references appear in the supplemental information: Bialy and Waldmann (2004); Minakawa et al. (2003); Oka et al. (2014, 2021); Watanabe et al. (1997).

REFERENCES

Amberger, J., Bocchini, C.A., Scott, A.F., and Hamosh, A. (2009). McKusick's online mendelian inheritance in man (OMIM). Nucleic Acids Res. *37*, D793–D796.

Amos, J.S., Huang, L., Thevenon, J., Kariminedjad, A., Beaulieu, C.L., Masurel-Paulet, A., Najmabadi, H., Fattahi, Z., Beheshtian, M., Tonekaboni, S.H., et al.; Care4Rare Canada Consortium (2017). Autosomal recessive mutations in *THOC6* cause intellectual disability: syndrome delineation requiring forward and reverse phenotyping. Clin. Genet. *91*, 92–99.

Ayyappan, V., Wat, R., Barber, C., Vivelo, C.A., Gauch, K., Visanpattanasin, P., Cook, G., Sazeides, C., and Leung, A.K.L. (2021). ADPriboDB 2.0: an updated database of ADP-ribosylated proteins. Nucleic Acids Res. *49* (D1), D261–D265.

Barthelmes, H.U., Habermeyer, M., Christensen, M.O., Mielke, C., Interthal, H., Pouliot, J.J., Boege, F., and Marko, D. (2004). TDP1 overexpression in human cells counteracts DNA damage mediated by topoisomerases I and II. J. Biol. Chem. *279*, 55618–55625.

Bartlett, E., Bonfiglio, J.J., Prokhorova, E., Colby, T., Zobel, F., Ahel, I., and Matic, I. (2018). Interplay of histone marks with serine ADP-ribosylation. Cell Rep. *24*, 3488–3502.e5.

Bialy, L., and Waldmann, H. (2004). Total synthesis and biological evaluation of the protein phosphatase 2A inhibitor cytostatin and analogues. Chemistry *10*, 2759–2780.

Blum, M., Chang, H.Y., Chuguransky, S., Grego, T., Kandasaamy, S., Mitchell, A., Nuka, G., Paysan-Lafosse, T., Qureshi, M., Raj, S., et al. (2021). The InterPro protein families and domains database: 20 years on. Nucleic Acids Res. *49* (D1), D344–D354.

Bohl, J., Brimer, N., Lyons, C., and Vande Pol, S.B. (2007). The stardust family protein MPP7 forms a tripartite complex with LIN7 and DLG1 that regulates the stability and localization of DLG1 to cell junctions. J. Biol. Chem. *282*, 9392–9400.

Bonfiglio, J.J., Colby, T., and Matic, I. (2017). Mass spectrometry for serine ADP-ribosylation? Think o-glycosylation! Nucleic Acids Res. *45*, 6259–6264.

Buch-Larsen, S.C., Hendriks, I.A., Lodge, J.M., Rykær, M., Furtwängler, B., Shishkova, E., Westphall, M.S., Coon, J.J., and Nielsen, M.L. (2020). Mapping physiological ADP-ribosylation using activated ion electron transfer dissociation. Cell Rep. *32*, 108176.

Campalans, A., Kortulewski, T., Amouroux, R., Menoni, H., Vermeulen, W., and Radicella, J.P. (2013). Distinct spatiotemporal patterns and PARP dependence of XRCC1 recruitment to single-strand break and base excision repair. Nucleic Acids Res. *41*, 3115–3129.

Chen, H., Li, Y., Zhang, J., Ran, Y., Wei, J., Yang, Y., and Shu, H.B. (2013). RAVER1 is a coactivator of MDA5-mediated cellular antiviral response. J. Mol. Cell Biol. *5*, 111–119.

Cho, H., and Kehrl, J.H. (2007). Localization of Gi α proteins in the centrosomes and at the midbody: implication for their role in cell division. J. Cell Biol. *178*, 245–255.

Conibear, A.C. (2020). Deciphering protein post-translational modifications using chemical biology tools. Nat. Rev. Chem. *4*, 674–695.

Cox, J., and Mann, M. (2008). MaxQuant enables high peptide identification rates, individualized p.p.b.-range mass accuracies and proteome-wide protein quantification. Nat. Biotechnol. *26*, 1367–1372.

Cox, J., and Mann, M. (2012). 1D and 2D annotation enrichment: a statistical method integrating quantitative proteomics with complementary high-throughput data. BMC Bioinformatics. *16*, S12.

Crawford, K., Bonfiglio, J.J., Mikoč, A., Matic, I., and Ahel, I. (2018). Specificity of reversible ADP-ribosylation and regulation of cellular processes. Crit. Rev. Biochem. Mol. Biol. *53*, 64–82.

DaRosa, P.A., Wang, Z., Jiang, X., Pruneda, J.N., Cong, F., Klevit, R.E., and Xu, W. (2015). Allosteric activation of the RNF146 ubiquitin ligase by a poly(ADP-ribosyl)ation signal. Nature *517*, 223–226.

Dasovich, M., Beckett, M.Q., Bailey, S., Ong, S.E., Greenberg, M.M., and Leung, A.K.L. (2021). Identifying poly(ADP-ribose)-binding proteins with photoaffinity-based proteomics. J. Am. Chem. Soc. *143*, 3037–3042.

de Castro, E., Sigrist, C.J.A., Gattiker, A., Builliard, V., Langendijk-Genevaux, P.S., Gasteiger, E., Bairoch, A., and Hulo, N. (2006). ScanProsite: detection of PROSITE signature matches and ProRule-associated functional and structural residues in proteins. Nucleic Acids Res. *34*, W362–W365.

Fahrer, J., Kranaster, R., Altmeyer, M., Marx, A., and Bürkle, A. (2007). Quantitative analysis of the binding affinity of poly(ADP-ribose) to specific binding proteins as a function of chain length. Nucleic Acids Res. *35*, e143.

Fahrer, J., Popp, O., Malanga, M., Beneke, S., Markovitz, D.M., Ferrando-May, E., Bürkle, A., and Kappes, F. (2010). High-affinity interaction of poly(ADP-ribose) and the human DEK oncoprotein depends upon chain length. Biochemistry *49*, 7119–7130.

Fan, H., Lu, J., Guo, Y., Li, D., Zhang, Z.M., Tsai, Y.H., Pi, W.C., Ahn, J.H., Gong, W., Xiang, Y., et al. (2020). BAHCC1 binds H3K27me3 via a conserved BAH module to mediate gene silencing and oncogenesis. Nat. Genet. *52*, 1384–1396.

Fehr, A.R., Jankevicius, G., Ahel, I., and Perlman, S. (2018). Viral macrodomains: unique mediators of viral replication and pathogenesis. Trends Microbiol. *26*, 598–610.

Fei, J., Ishii, H., Hoeksema, M.A., Meitinger, F., Kassavetis, G.A., Glass, C.K., Ren, B., and Kadonaga, J.T. (2018). NDF, a nucleosome-destabilizing factor that facilitates transcription through nucleosomes. Genes Dev. *32*, 682–694.

Gagné, J.-P., Isabelle, M., Lo, K.S., Bourassa, S., Hendzel, M.J., Dawson, V.L., Dawson, T.M., and Poirier, G.G. (2008). Proteome-wide identification of poly(ADP-ribose) binding proteins and poly(ADP-ribose)-associated protein complexes. Nucleic Acids Res. *36*, 6959–6976.

Gibson, B.A., and Kraus, W.L. (2012). New insights into the molecular and cellular functions of poly(ADP-ribose) and PARPs. Nat. Rev. Mol. Cell Biol. *13*, 411–424.

Golan, T., Hammel, P., Reni, M., Van Cutsem, E., Macarulla, T., Hall, M.J., Park, J.O., Hochhauser, D., Arnold, D., Oh, D.Y., et al. (2019). Maintenance olaparib for germline *BRCA*-mutated metastatic pancreatic cancer. N. Engl. J. Med. *381*, 317–327.

Gräwe, C., Makowski, M.M., and Vermeulen, M. (2020). PAQMAN: protein-nucleic acid affinity quantification by MAss spectrometry in nuclear extracts. Methods *184*, 70–77.

Grunewald, M.E., Chen, Y., Kuny, C., Maejima, T., Lease, R., Ferraris, D., Aikawa, M., Sullivan, C.S., Perlman, S., and Fehr, A.R. (2019). The coronavirus macrodomain is required to prevent PARP-mediated inhibition of virus replication and enhancement of IFN expression. PLoS Pathog. *15*, e1007756.

Gu, Z., Eils, R., and Schlesner, M. (2016). Complex heatmaps reveal patterns and correlations in multidimensional genomic data. Bioinformatics *32*, 2847–2849.

Guo, J., and Zhang, J. (2020). Ubiquitination and deubiquitination in melanoma research and clinically relevant outcomes. In Ubiquitin-Proteasome Pathway, X. Zhan, ed. (IntechOpen). https://doi.org/10.5772/intechopen.94512 https://www.intechopen.com/chapters/73937.

Gupte, R., Liu, Z., and Kraus, W.L. (2017). PARPs and ADP-ribosylation: recent advances linking molecular functions to biological outcomes. Genes Dev. *31*, 101–126.

Hendriks, I.A., Larsen, S.C., and Nielsen, M.L. (2019). An advanced strategy for comprehensive profiling of ADP-ribosylation sites using mass spectrometry-based proteomics. Mol. Cell. Proteomics *18*, 1010–1026.

Heublein, M., Burguillos, M.A., Vögtle, F.N., Teixeira, P.F., Imhof, A., Meisinger, C., and Ott, M. (2014). The novel component Kgd4 recruits the E3 subunit to the mitochondrial α-ketoglutarate dehydrogenase. Mol. Biol. Cell *25*, 3342–3349.

Hoch, N.C., and Polo, L.M. (2019). ADP-ribosylation: from molecular mechanisms to human disease. Genet. Mol. Biol. *43* (1, suppl 1), e20190075.

Hottiger, M.O. (2015). Nuclear ADP-ribosylation and its role in chromatin plasticity, cell differentiation, and epigenetics. Annu. Rev. Biochem. *84*, 227–263.

Hsu, C.-L., Liu, J.S., Wu, P.L., Guan, H.H., Chen, Y.L., Lin, A.C., Ting, H.J., Pang, S.T., Yeh, S.D., Ma, W.L., et al. (2014). Identification of a new androgen receptor (AR) co-regulator BUD31 and related peptides to suppress wild-type and mutated AR-mediated prostate cancer growth via peptide screening and X-ray structure analysis. Mol. Oncol. *8*, 1575–1587.

Huang, W., Sherman, B.T., and Lempicki, R.A. (2009a). Bioinformatics enrichment tools: paths toward the comprehensive functional analysis of large gene lists. Nucleic Acids Res. *37*, 1–13.

Huang, W., Sherman, B.T., and Lempicki, R.A. (2009b). Systematic and integrative analysis of large gene lists using DAVID bioinformatics resources. Nat. Protoc. *4*, 44–57.

Jiang, G., and Sancar, A. (2006). Recruitment of DNA damage checkpoint proteins to damage in transcribed and nontranscribed sequences. Mol. Cell. Biol. *26*, 39–49.

Jungmichel, S., Rosenthal, F., Altmeyer, M., Lukas, J., Hottiger, M.O., and Nielsen, M.L. (2013). Proteome-wide identification of poly(ADP-Ribosyl)ation targets in different genotoxic stress responses. Mol. Cell *52*, 272–285.

Kalesh, K., Lukauskas, S., Borg, A.J., Snijders, A.P., Ayyappan, V., Leung, A.K.L., Haskard, D.O., and DiMaggio, P.A. (2019). An integrated chemical proteomics approach for quantitative profiling of intracellular ADP-ribosylation. Sci. Rep. *9*, 6655.

Kamaletdinova, T., Fanaei-Kahrani, Z., and Wang, Z.-Q. (2019). The enigmatic function of PARP1: from parylation activity to PAR readers. Cells *8*, E1625.

Kang, H.C., Lee, Y.I., Shin, J.H., Andrabi, S.A., Chi, Z., Gagné, J.P., Lee, Y., Ko, H.S., Lee, B.D., Poirier, G.G., et al. (2011). Iduna is a poly(ADP-ribose) (PAR)-dependent E3 ubiquitin ligase that regulates DNA damage. Proc. Natl. Acad. Sci. USA *108*, 14103–14108.

Karlberg, T., Langelier, M.F., Pascal, J.M., and Schüler, H. (2013). Structural biology of the writers, readers, and erasers in mono- and poly(ADP-ribose) mediated signaling. Mol. Aspects Med. *34*, 1088–1108.

Khoury-Haddad, H., Guttmann-Raviv, N., Ipenberg, I., Huggins, D., Jeyasekharan, A.D., and Ayoub, N. (2014). PARP1-dependent recruitment of KDM4D histone demethylase to DNA damage sites promotes double-strand break repair. Proc. Natl. Acad. Sci. USA *111*, E728–E737.

Khoury-Haddad, H., Nadar-Ponniah, P.T., Awwad, S., and Ayoub, N. (2015). The emerging role of lysine demethylases in DNA damage response: dissecting the recruitment mode of KDM4D/JMJD2D to DNA damage sites. Cell Cycle *14*, 950–958.

Kim, D.-S., Challa, S., Jones, A., and Kraus, W.L. (2020). PARPs and ADP-ribosylation in RNA biology: from RNA expression and processing to protein translation and proteostasis. Genes Dev. *34*, 302–320.

Kistemaker, H.A.V., Lameijer, L.N., Meeuwenoord, N.J., Overkleeft, H.S., van der Marel, G.A., and Filippov, D.V. (2015). Synthesis of well-defined adenosine diphosphate ribose oligomers. Angew. Chem. Int. Ed. Engl. *54*, 4915–4918.

Kistemaker, H.A.V., Nardozza, A.P., Overkleeft, H.S., van der Marel, G.A., Ladurner, A.G., and Filippov, D.V. (2016). Synthesis and macrodomain binding of mono-ADP-ribosylated peptides. Angew. Chem. Int. Ed. Engl. *55*, 10634–10638.

Kliza, K., Taumer, C., Pinzuti, I., Franz-Wachtel, M., Kunzelmann, S., Stieglitz, B., Macek, B., and Husnjak, K. (2017). Internally tagged ubiquitin: a tool to identify linear polyubiquitin-modified proteins by mass spectrometry. Nat. Methods *14*, 504–512.

Krietsch, J., Rouleau, M., Pic, É., Ethier, C., Dawson, T.M., Dawson, V.L., Masson, J.Y., Poirier, G.G., and Gagné, J.P. (2013). Reprogramming cellular events by poly(ADP-ribose)-binding proteins. Mol. Aspects Med. *34*, 1066–1087.

Laly, A.C., Sliogeryte, K., Pundel, O.J., Ross, R., Keeling, M.C., Avisetti, D., Waseem, A., Gavara, N., and Connelly, J.T. (2021). The keratin network of intermediate filaments regulates keratinocyte rigidity sensing and nuclear mechanotransduction. Sci. Adv. *7*, eabd6187.

Lam, A.T., Zhang, X.N., Courouble, V.V., Strutzenberg, T.S., Pei, H., Stiles, B.L., Louie, S.G., Griffin, P.R., and Zhang, Y. (2021). A bifunctional NAD^+ for profiling poly-ADP-ribosylation-dependent interacting proteins. ACS Chem. Biol. *16*, 389–396.

Lambrecht, M.J., Brichacek, M., Barkauskaite, E., Ariza, A., Ahel, I., and Hergenrother, P.J. (2015). Synthesis of dimeric ADP-ribose and its structure with human poly(ADP-ribose) glycohydrolase. J. Am. Chem. Soc. *137*, 3558–3564.

Larsen, S.C., Hendriks, I.A., Lyon, D., Jensen, L.J., and Nielsen, M.L. (2018). Systems-wide analysis of serine ADP-ribosylation reveals widespread occurrence and site-specific overlap with phosphorylation. Cell Rep. *24*, 2493–2505.e4.

Lin, H. (2007). Nicotinamide adenine dinucleotide: beyond a redox coenzyme. Org. Biomol. Chem. *5*, 2541–2554.

Liu, Q., Kistemaker, H.A.V., Bhogaraju, S., Dikic, I., Overkleeft, H.S., van der Marel, G.A., Ovaa, H., van der Heden van Noort, G.J., and Filippov, D.V. (2018). A general approach towards triazole-linked adenosine diphosphate ribosylated peptides and proteins. Angew. Chem. Int. Ed. Engl. *57*, 1659–1662.

Liu, Q., van der Marel, G.A., and Filippov, D.V. (2019). Chemical ADP-ribosylation: mono-ADPr-peptides and oligo-ADP-ribose. Org. Biomol. Chem. *17*, 5460–5474.

Longo, P.A., Kavran, J.M., Kim, M.-S., and Leahy, D.J. (2013). Transient mammalian cell transfection with polyethylenimine (PEI). Methods Enzymol. *529*, 227–240.

Lüscher, B., Bütepage, M., Eckei, L., Krieg, S., Verheugd, P., and Shilton, B.H. (2018). ADP-ribosylation, a multifaceted posttranslational modification involved in the control of cell physiology in health and disease. Chem. Rev. *118*, 1092–1136.

Makowski, M.M., Gräwe, C., Foster, B.M., Nguyen, N.V., Bartke, T., and Vermeulen, M. (2018). Global profiling of protein-DNA and protein-nucleosome binding affinities using quantitative mass spectrometry. Nat. Commun. *9*, 1653.

Marneros, A.G. (2013). BMS1 is mutated in aplasia cutis congenita. PLoS Genet. *9*, e1003573.

Martello, R., Leutert, M., Jungmichel, S., Bilan, V., Larsen, S.C., Young, C., Hottiger, M.O., and Nielsen, M.L. (2016). Proteome-wide identification of the endogenous ADP-ribosylome of mammalian cells and tissue. Nat. Commun. *7*, 12917.

Martin, K.A., Cesaroni, M., Denny, M.F., Lupey, L.N., and Tempera, I. (2015). Global transcriptome analysis reveals that poly(ADP-ribose) polymerase 1 regulates gene expression through EZH2. Mol. Cell. Biol. *35*, 3934–3944.

Mattioli, F., Isidor, B., Abdul-Rahman, O., Gunter, A., Huang, L., Kumar, R., Beaulieu, C., Gecz, J., Innes, M., Mandel, J.L., and Piton, A. (2019). Clinical and functional characterization of recurrent missense variants implicated in *THOC6*-related intellectual disability. Hum. Mol. Genet. *28*, 952–960.

McGurk, L., Rifai, O.M., and Bonini, N.M. (2019). Poly(ADP-ribosylation) in age-related neurological disease. Trends Genet. *35*, 601–613.

Minakawa, N., Kato, Y., Uetake, K., Kaga, D., and Matsuda, A. (2003). An improved large scale synthesis of 1,4-anhydro-4-thio-d-ribitol. Tetrahedron *59*, 1699–1702.

Minchom, A., Aversa, C., and Lopez, J. (2018). Dancing with the DNA damage response: next-generation anti-cancer therapeutic strategies. Ther. Adv. Med. Oncol. *10*, 1758835918786658.

Nagaraj, N., Wisniewski, J.R., Geiger, T., Cox, J., Kircher, M., Kelso, J., Pääbo, S., and Mann, M. (2011). Deep proteome and transcriptome mapping of a human cancer cell line. Mol. Syst. Biol. *7*, 548.

Ohbayashi, N., and Fukuda, M. (2020). Recent advances in understanding the molecular basis of melanogenesis in melanocytes. F1000Res. *9*, 608.

Oka, N., Kajino, R., Takeuchi, K., Nagakawa, H., and Ando, K. (2014). α-Selective ribofuranosylation of alcohols with ribofuranosyl iodides and triphenylphosphine oxide. J. Org. Chem. *79*, 7656–7664.

Oka, N., Mori, A., Suzuki, K., and Ando, K. (2021). Stereoselective synthesis of ribofuranoid *exo*-glycals by one-pot Julia olefination using ribofuranosyl sulfones. J. Org. Chem. *86*, 657–673.

Olivieri, M., Cho, T., Álvarez-Quilón, A., Li, K., Schellenberg, M.J., Zimmermann, M., Hustedt, N., Rossi, S.E., Adam, S., Melo, H., et al. (2020). A genetic map of the response to DNA damage in human cells. Cell *182*, 481–496.e21.

Palazzo, L., Leidecker, O., Prokhorova, E., Dauben, H., Matic, I., and Ahel, I. (2018). Serine is the major residue for ADP-ribosylation upon DNA damage. eLife *7*, e34334.

Palazzo, L., Mikolčević, P., Mikoč, A., and Ahel, I. (2019). ADP-ribosylation signalling and human disease. Open Biol. *9*, 190041.

Patel, M., Nowsheen, S., Maraboyina, S., and Xia, F. (2020). The role of poly(ADP-ribose) polymerase inhibitors in the treatment of cancer and methods to overcome resistance: a review. Cell Biosci. *10*, 35.

Perez-Riverol, Y., Csordas, A., Bai, J., Bernal-Llinares, M., Hewapathirana, S., Kundu, D.J., Inuganti, A., Griss, J., Mayer, G., Eisenacher, M., et al. (2019). The PRIDE database and related tools and resources in 2019: improving support for quantification data. Nucleic Acids Res. *47* (D1), D442–D450.

Pignochino, Y., Capozzi, F., D'Ambrosio, L., Dell'Aglio, C., Basiricò, M., Canta, M., Lorenzato, A., Vignolo Lutati, F., Aliberti, S., Palesandro, E., et al. (2017). PARP1 expression drives the synergistic antitumor activity of trabectedin and PARP1 inhibitors in sarcoma preclinical models. Mol. Cancer *16*, 86.

Piñero, J., et al. (2019). The DisGeNET knowledge platform for disease genomics: 2019 update. Nucleic Acids Res. *48* (D1), D845–D855.

Pleschke, J.M., Kleczkowska, H.E., Strohm, M., and Althaus, F.R. (2000). Poly(ADP-ribose) binds to specific domains in DNA damage checkpoint proteins. J. Biol. Chem. *275*, 40974–40980.

Pühringer, T., Hohmann, U., Fin, L., Pacheco-Fiallos, B., Schellhaas, U., Brennecke, J., and Plaschka, C. (2020). Structure of the human core transcription-export complex reveals a hub for multivalent interactions. eLife *9*, e61503.

Rappsilber, J., Mann, M., and Ishihama, Y. (2007). Protocol for micro-purification, enrichment, pre-fractionation and storage of peptides for proteomics using StageTips. Nat. Protoc. *2*, 1896–1906.

Ray Chaudhuri, A., and Nussenzweig, A. (2017). The multifaceted roles of PARP1 in DNA repair and chromatin remodelling. Nat. Rev. Mol. Cell Biol. *18*, 610–621.

Rimar, K.J., Tran, P.T., Matulewicz, R.S., Hussain, M., and Meeks, J.J. (2017). The emerging role of homologous recombination repair and PARP inhibitors in genitourinary malignancies. Cancer *123*, 1912–1924.

Ryu, K.W., Kim, D.-S., and Kraus, W.L. (2015). New facets in the regulation of gene expression by ADP-ribosylation and poly(ADP-ribose) polymerases. Chem. Rev. *115*, 2453–2481.

Shamseldin, H.E., Makhseed, N., Ibrahim, N., Al-Sheddi, T., Alobeid, E., Abdulwahab, F., and Alkuraya, F.S. (2019). NUP214 deficiency causes severe encephalopathy and microcephaly in humans. Hum. Genet. *138*, 221–229.

Shin, C., Ito, Y., Ichikawa, S., Tokunaga, M., Sakata-Sogawa, K., and Tanaka, T. (2017). MKRN2 is a novel ubiquitin E3 ligase for the p65 subunit of NF-κB and negatively regulates inflammatory responses. Sci. Rep. *7*, 46097.

Skruber, K., Warp, P.V., Shklyarov, R., Thomas, J.D., Swanson, M.S., Henty-Ridilla, J.L., Read, T.A., and Vitriol, E.A. (2020). Arp2/3 and Mena/VASP require profilin 1 for actin network assembly at the leading edge. Curr. Biol. *30*, 2651–2664.e5.

Spruijt, C.G., Gnerlich, F., Smits, A.H., Pfaffeneder, T., Jansen, P.W., Bauer, C., Münzel, M., Wagner, M., Müller, M., Khan, F., et al. (2013). Dynamic readers for 5-(hydroxy)methylcytosine and its oxidized derivatives. Cell *152*, 1146–1159.

Teloni, F., and Altmeyer, M. (2016). Readers of poly(ADP-ribose): designed to be fit for purpose. Nucleic Acids Res. *44*, 993–1006.

Tillotson, R., Selfridge, J., Koerner, M.V., Gadalla, K.K.E., Guy, J., De Sousa, D., Hector, R.D., Cobb, S.R., and Bird, A. (2017). Radically truncated MeCP2 rescues Rett syndrome-like neurological defects. Nature *550*, 398–401.

Tyanova, S., Temu, T., Sinitcyn, P., Carlson, A., Hein, M.Y., Geiger, T., Mann, M., and Cox, J. (2016). The Perseus computational platform for comprehensive analysis of (prote)omics data. Nat. Methods *13*, 731–740.

van der Heden, van Noort, G.J., van der Horst, M.G., Overkleeft, H.S., van der Marel, G.A., and Filippov, D.V. (2010). Synthesis of mono-ADP-ribosylated oligopeptides using ribosylated amino acid building blocks. J. Am. Chem. Soc. *132*, 5236–5240.

van Zon, A., Mossink, M.H., Schoester, M., Houtsmuller, A.B., Scheffer, G.L., Scheper, R.J., Sonneveld, P., and Wiemer, E.A. (2003). The formation of vault-tubes: a dynamic interaction between vaults and vault PARP. J. Cell Sci. *116*, 4391–4400.

Voorneveld, J., Rack, J.G.M., Ahel, I., Overkleeft, H.S., van der Marel, G.A., and Filippov, D.V. (2018). Synthetic α- and β-Ser-ADP-ribosylated peptides reveal α-Ser-ADPr as the native epimer. Org. Lett. *20*, 4140–4143.

Wang, Y., Kim, N.S., Haince, J.F., Kang, H.C., David, K.K., Andrabi, S.A., Poirier, G.G., Dawson, V.L., and Dawson, T.M. (2011). Poly(ADP-ribose) (PAR) binding to apoptosis-inducing factor is critical for PAR polymerase-1-dependent cell death (parthanatos). Sci. Signal. *4*, ra20.

Watanabe, Y., Nakamura, T., and Mitsumoto, H. (1997). Protection of phosphate with the 9-fluorenylmethyl group. Synthesis of unsaturated-acyl phosphatidylinositol 4,5-bisphosphate. Tetrahedron Lett. *38*, 7407–7410.

Waterhouse, A.M., Procter, J.B., Martin, D.M., Clamp, M., and Barton, G.J. (2009). Jalview version 2—a multiple sequence alignment editor and analysis workbench. Bioinformatics *25*, 1189–1191.

Wiśniewski, J.R., Zougman, A., Nagaraj, N., and Mann, M. (2009). Universal sample preparation method for proteome analysis. Nat. Methods *6*, 359–362.

Yamaguchi, H., Yoshida, S., Muroi, E., Kawamura, M., Kouchi, Z., Nakamura, Y., Sakai, R., and Fukami, K. (2010). Phosphatidylinositol 4,5-bisphosphate and PIP5-kinase Iα are required for invadopodia formation in human breast cancer cells. Cancer Sci. *101*, 1632–1638.

Zhang, X., Smits, A.H., van Tilburg, G.B., Jansen, P.W., Makowski, M.M., Ovaa, H., and Vermeulen, M. (2017). An Interaction Landscape of Ubiquitin Signaling. Mol. Cell *65*, 941–955.e8.

Zhang, Q., Mady, A.S.A., Ma, Y., Ryan, C., Lawrence, T.S., Nikolovska-Coleska, Z., Sun, Y., and Morgan, M.A. (2019). The WD40 domain of FBXW7 is a poly(ADP-ribose)-binding domain that mediates the early DNA damage response. Nucleic Acids Res. *47*, 4039–4053.

Zhen, Y., Zhang, Y., and Yu, Y. (2017). A cell-line-specific atlas of PARP-mediated protein Asp/Glu-ADP-ribosylation in breast cancer. Cell Rep. *21*, 2326–2337.

STAR★METHODS

KEY RESOURCES TABLE

REAGENT or RESOURCE	SOURCE	IDENTIFIER
Antibodies		
Mouse monoclonal anti-XRCC1	Santa Cruz Biotechnology	Cat#sc-56254; RRID: AB_794191
Mouse monoclonal anti-ATR	Santa Cruz Biotechnology	Cat#sc-515173; RRID: AB_2893291
Mouse monoclonal anti-DLD	Santa Cruz Biotechnology	Cat#sc-365977; RRID: AB_10917587
Rabbit monoclonal anti-GAPDH	Cell Signaling Technology	Cat#2118S; RRID: AB_561053
Mouse monoclonal anti-IMPDH	Santa Cruz Biotechnology	Cat#sc-166551; RRID: AB_2127354
Mouse monoclonal anti-KIF14	Santa Cruz Biotechnology	Cat#sc-365553; RRID: AB_10847216
Mouse monoclonal anti-ME2	Santa Cruz Biotechnology	Cat#sc-514850; RRID: AB_2893292
Mouse monoclonal anti-MKRN2	Santa Cruz Biotechnology	Cat#sc-514185; RRID: AB_2893293
Rabbit polyclonal anti-MKRN2	Abcam	Cat#ab72055; RRID: AB_1269435
Mouse monoclonal anti-MVP/LRP	Santa Cruz Biotechnology	Cat#sc-23916; RRID: AB_627891
Mouse monoclonal anti-NOLC1/NOPP140	Santa Cruz Biotechnology	Cat#sc-374033; RRID: AB_10917069
Mouse monoclonal anti-SFPQ/PSF	Santa Cruz Biotechnology	Cat#sc-374502; RRID: AB_10989589
Mouse monoclonal anti-TDP1	Santa Cruz Biotechnology	Cat#sc-365674; RRID: AB_10847225
Mouse monoclonal anti-THOC1	Santa Cruz Biotechnology	Cat#sc-514123; RRID: AB_2893294
Mouse monoclonal anti-THOC5/FMIP	Santa Cruz Biotechnology	Cat#sc-514146; RRID: AB_2893295
Mouse monoclonal anti-THOC6	Santa Cruz Biotechnology	Cat#sc-390722; RRID: AB_2893296
Rabbit polyclonal anti-ZC3H14	Biorbyt	Cat#orb422692; RRID: AB_2893297
Rabbit polyclonal anti-MACROD1	NOVUS BIOLOGICALS	Cat#NBP2-85248; RRID: AB_2893298
Rabbit polyclonal anti-OGFR	NOVUS BIOLOGICALS	Cat#NBP2-83799; RRID: AB_2893299
Mouse monoclonal anti-TUBA1A	Thermo Fisher Scientific	Cat#T5168; RRID: AB_477579
Mouse monoclonal anti-GST	Santa Cruz Biotechnology	Cat#sc-138; RRID: AB_627677
Rabbit polyclonal anti-HIS	Cell Signaling Technology	Cat#CST 2365T; RRID: AB_2115720
Mouse monoclonal anti-Ub (P4D1)	Santa Cruz Biotechnology	Cat#Sc-8017; RRID: AB_628423
Rabbit polyclonal anti-Streptavidin-HRP conjugated	Thermo Fisher Scientific	Cat#PA1-26848 ; RRID: AB_795453
Rabbit monoclonal anti-H2AX	Cell Signaling Technology	Cat#7631S; RRID: AB_10860771
Rabbit monoclonal anti-γH2AX	Cell Signaling Technology	Cat#9718S; RRID: AB_2118009
Rabbit polyclonal anti-GFP	Abcam	Cat#ab290; RRID: AB_303395
Mouse monoclonal anti-FLAG (M2)	Sigma-Aldrich	Cat#F3165; RRID: AB_259529
Mouse monoclonal anti-C-MYC	Santa Cruz Biotechnology	Cat#sc-40; RRID: AB_2857941
Chemicals, peptides, and recombinant proteins		
Biotin-monoADPr probe	This paper	N/A
Biotin-diADPr probe	This paper	N/A
Biotin-triADPr probe	This paper	N/A
Untagged monoADPr	This paper	N/A
Untagged triADPr probe	This paper	N/A
Unfractionated PAR polymer	Trevigen	Cat#4336-100-02
Biotin-triA	Integrated DNA Technologies	N/A
Biotin-pentadecaA	Integrated DNA Technologies	N/A
$MgCl_2$-ATP Solution	BostonBiochem	Cat#B-20
PDD00017273 (PARG inhibitor)	TOCRIS	Cat#5952/10
Olaparib (AZD2281, KU-0059436)	Selleckchem	Cat#S1060
PhosSTOP	Sigma-Aldrich	Cat#4906837001

(*Continued on next page*)

Continued

REAGENT or RESOURCE	SOURCE	IDENTIFIER
Hydrogen peroxide	Sigma-Aldrich	Cat#H1009
cOmplete Protease Inhibitor Cocktail	Sigma-Aldrich	Cat#4693132001
N-Ethylmaleimide	Sigma-Aldrich	Cat#E3876
Iodoacetamide	Sigma-Aldrich	Cat#I1149
TrypLE Express Enzyme (1X), phenol red	Thermo Fisher Scientific	Cat#12605028
Trypsin	Promega	Cat#V5280
Polyethylenimine	Sigma-Aldrich	Cat#408727
TCEP	Sigma-Aldrich	Cat#646547
Benzonase nuclease	Sigma-Aldrich	Cat#1016970001
Recombinant ENPP1	R&D Systems	Cat#6136-EN-010
Recombinant PARG	Enzo Life Sciences	Cat#ALX-202-045-UC01
Recombinant E1 (UBE1)	BostonBiochem	Cat#E-304-050
Recombinant E2 (UbcH5a/UBE2D1)	BostonBiochem	Cat#E2-616-100
Recombinant Ub	BostonBiochem	Cat#U-100H
Recombinant MKRN2-GST	Abnova	Cat#H00023609-P01
Recombinant MECP2-GST	Abnova	Cat#H00004204-P01
Recombinant THOC6/WDR58-GST	Abnova	Cat#H00079228-P02
Recombinant XRCC1-GST	Abnova	Cat#H00007515-P01
Recombinant GST-HIS	Mybiosource	Cat#MBS143838
Recombinant IMPDH-6xHIS	Origene	Cat#AR50099PU-S
Streptavidin Sepharose	GE healthcare Life Sciences	Cat#17-5113-01
Dynabeads MyOne Streptavidin C1	Thermo Fisher Scientific	Cat#65001
Critical commercial assays		
QuikChange II Site-Directed Mutagenesis Kit	Agilent	Cat#200523
Pierce BCA Protein Assay Kit	Thermo Fisher Scientific	Cat#23225
Deposited data		
MS raw and analyzed data	This paper	PXD: PXD024233
Immunobloting raw data	This paper	Mendeley Data: https://doi.org/10.17632/f278t3f4dx.1
Experimental models: Cell lines		
HeLa	Spruijt et al., 2013	N/A
HaCaT	Laboratory of Michiel Vermeulen	N/A
Oligonucleotides		
See Table S2 for the list of primers used to generate mutants of MVP, TDP1 and MKRN2		N/A
Recombinant DNA		
pcDNA3-Flag ATR	Jiang and Sancar, 2006	Addgene: Cat#31611
pEGFP-N1 MeCP2	Tillotson et al., 2017	Addgene: Cat#110186
pEGFP-NI XRCC1	Campalans et al., 2013	N/A
pMC-EGFPP-N TDP1	Barthelmes et al., 2004	N/A
pMC-EGFPP-N TDP1 (1-153)	This paper	N/A
pMC-EGFPP-N TDP1 (1-164)	This paper	N/A
pMC-EGFPP-N TDP1 (1-587)	This paper	N/A
p3xFLAG-CMV BUD31	Hsu et al., 2014	N/A
pFLAG MPP7	Bohl et al., 2007	N/A
MYC-LIN7C	Bohl et al., 2007	N/A

(*Continued on next page*)

Continued

REAGENT or RESOURCE	SOURCE	IDENTIFIER
pEGFP mPIP5KIβ	Yamaguchi et al., 2010	N/A
pEGFP-N1 MVP	van Zon et al., 2003	N/A
pEGFP-N1 MVP R507A	This paper	N/A
pEGFP-N1 MVP R511A	This paper	N/A
pEGFP-N1 MVP R512A	This paper	N/A
pEGFP-N1 MVP R507/511A	This paper	N/A
pEGFP-N1 MVP R507/512A	This paper	N/A
pEGFP-N1 MVP R511/512A	This paper	N/A
pEGFP-N1 MVP R507/511/512A	This paper	N/A
pCMV-Flag mMKRN2	Shin et al., 2017	N/A
pCMV-Flag mMKRN2 (1-164)	This paper	N/A
pCMV-Flag mMKRN2 (1-194)	This paper	N/A
pCMV-Flag mMKRN2 (1-237)	This paper	N/A
pCMV-Flag mMKRN2 (1-321)	This paper	N/A
pCMV-Flag mMKRN2 (1-352)	This paper	N/A
Software and algorithms		
ImageJ/Fiji	NIH	https://imagej.net/software/fiji/
MaxQuant (1.5.0.1)	Cox and Mann, 2008	https://www.biochem.mpg.de/5111795/maxquant
Perseus (1.5.0.15)	Cox and Mann, 2012	https://www.biochem.mpg.de/5111810/perseus
R (3.4.1)	R project	https://www.r-project.org
Proteome Discoverer 2.2	Thermo Fisher Scientific	
Python (3.7)	Python Software Foundation. Python Language Reference.	https://www.python.org
DAVID Bioinformatics Resources 6.8	Huang et al., 2009a, 2009b	https://david.ncifcrf.gov
ScanProsite	de Castro et al., 2006	https://www.expasy.org/tools/scanprosite/
InterPro	Blum et al., 2021	https://www.ebi.ac.uk/interpro/
Online Mendelian Inheritance in Man, OMIM	Amberger et al., 2009	https://omim.org/
DisGeNET v7	Piñero et al., 2019	https://www.disgenet.org/
Jalview	Waterhouse et al., 2009	https://www.jalview.org/
Other		
Protein copy number dataset for HeLa cell line	Nagaraj et al., 2011	https://doi.org/10.1038/msb.2011.81
DDR network dataset used to generate Figure 6B	Olivieri et al., 2020	https://doi.org/10.1016/j.cell.2020.05.040

RESOURCE AVAILABILITY

Lead contact

Further information and requests for resources and reagents should be directed to and will be fulfilled by the lead contact Michiel Vermeulen (Michiel.Vermeulen@science.ru.nl).

Materials availability

All unique/stable reagents generated in this study are available from the lead contact with a completed Materials Transfer Agreement.

Data and code availability

The mass spectrometry proteomics data generated during this study have been deposited to the ProteomeXchange Consortium via the PRIDE partner repository (Perez-Riverol et al., 2019) with the dataset identifier PXD: PXD024233. Original western blot images have been deposited at Mendeley and are publicly available as of the date of publication. The DOI is listed in the Key resources table.

This paper analyses existing, publicly available data. The accession numbers for the datasets are listed in the Key resources table.

This paper does not report original code.

Any additional information required to reanalyse the data reported in this paper is available from the lead contact upon request.

EXPERIMENTAL MODEL AND SUBJECT DETAILS

Cell culture

Human cervix adenocarcinoma HeLa and human epidermal keratinocyte HaCaT cells were cultured in Dulbecco's Modified Eagle's Medium (DMEM, Thermo) supplemented with 10% Fetal bovine serum (FBS, Hyclone) and 1% Penicillin/Streptomycin (15140-122, Thermo). Early passages of both cell lines were propagated and frozen at liquid nitrogen, and aliquots were used for a limited number of passages. Both cell lines tested negative for *Mycoplasma* contamination.

METHOD DETAILS

Drug treatment

To inhibit PARP activity, cells were treated with either DMSO (control) or Olaparib inhibitor (Selleckchem) at final concentration of 10 μM for 2 hours. To induce oxidative DNA damage, HeLa cells were first pre-treated with Olaparib, followed by stimulation with 2mM hydrogen peroxide (Sigma-Aldrich) for indicated time points (Bartlett et al., 2018).

Plasmid constructs

The pcDNA3-ATR WT -FLAG construct was provided by Aziz Sancar via Addgene (Cat#31611) as described in Jiang and Sancar (2006), whereas pEGFP-N1-MeCP2 was provided by Adrian Bird via Addgene (Cat#110186) as published in Tillotson et al. (2017). pEGFP-NI XRCC1 was a kind gift from Pablo Radicella (Campalans et al., 2013), pMC-EGFPP-N TDP1 was provided by Fritz Boege (Barthelmes et al., 2004), Cheng-Lung Hsu kindly provided p3xFLAG-CMV BUD31 plasmid (Hsu et al., 2014). pFLAG-MPP7 and plasmid encoding MYC-LIN7C were a kind gifts of Scott B. Vande Pol (Bohl et al., 2007), whereas pEGFP-mPIP5KIβ was provided by Yamaguchi et al. (2010). pEGFP-N1 MVP was kindly provided by Erik A.C. Wiemer (van Zon et al., 2003), whereas pCMV-Flag-mMKRN2 plasmid was a kind gift from Takashi Tanaka (Shin et al., 2017). Mutants of pEGFP-N1 MVP and truncated variants of pMC-EGFPP-N TDP1 and pCMV-Flag-mMKRN2 were generated using QuikChange II Site-Directed Mutagenesis Kit (Agilent) according to the manufacturer's instructions. All plasmids generated in this study are listed in Key resources table and all primers sequences are provided in Table S2.

The integrity of all constructs was verified by sequencing.

Plasmid DNA transfection

HeLa cells were transfected with either empty vector or indicated plasmids using Polyethylenimine (PEI, Sigma-Aldrich) (Longo et al., 2013). PEI was diluted in Opti-MEM medium and incubated at room temperature (RT) for 5 min. The plasmid DNA (typically between 200 ng and 2 μg) was also diluted in Opti-MEM medium. Next, the diluted PEI was added to diluted plasmid DNA at PEI:DNA ratio 3:1 and incubated at RT for 15 min. The PEI:DNA complex was added drop-wise to the cells. The medium containing transfection mixture was replaced with fresh DMEM medium after at least 18 h. 24-48 h post-infections cells were harvested and whole-cell extracts were prepared as described in Protein extract preparation section.

Protein extract preparation

Whole cell extracts for affinity purification experiments were prepared as described previously with certain modifications (Zhang et al., 2017). Briefly, cells were harvested by trypsinisation (trypsin, Promega) and cell pellet was washed thrice with ice-cold Olaparib-supplemented PBS. Cells were lysed in 5 cell pellet volumes of lysis buffer (50 mM Tris-HCl pH 8.0, 150 mM NaCl, 1.5 mM MgCl2, 0.5% (v/v) NP-40, 1 ul bensonase (Sigma-Aldrich), 1x cOmplete Protease Inhibitor Cocktail (Sigma-Aldrich), 1x PhosStop™ (Sigma-Aldrich), 10 μM Olaparib (Selleckchem), 2 mM NEM (Sigma-Aldrich) and 1 mM DTT). The cell suspension was passed several times through a syringe to mechanically disrupt cellular membranes. After 30 min incubation on rotation wheel at 4°C, lysate was centrifuged (12000 rpm, 30 min, 4°C). The supernatant was collected and passed through 0.22 μm syringe filter. The cleared whole-cell extract was supplemented with 10% (v/v) glycerol and snap frozen.

Nuclear extracts were prepared essentially as described (Spruijt et al., 2013). Briefly, HeLa and HaCaT cells were harvested by incubation with trypsin (Promega) and TrypLE Express Enzyme (1X, Thermo Fischer Scientific), respectively. Cells were wash twice in ice-cold PBS, followed by resuspension and incubation in 5 cell pellet volumes of Buffer A (10 mM HEPES KOH pH 7.9, 15 mM MgCl2, 10 mM KCl) for 10 min at 4°C. After centrifugation (400 g, 5 min, 4°C), cells were resuspended in 2 cell pellet volumes of Buffer A, supplemented with 0.15% NP-40, 1x cOmplete Protease Inhibitor Cocktail (Sigma-Aldrich), 1x PhosStop™ (Sigma-Aldrich), 10 μM Olaparib (Selleckchem) and 2 mM NEM (Sigma-Aldrich). Cells were lysed by dounce homogenization, followed by centrifugation (3200 g, 15 min, 4°C). Obtained crude nuclei were washed in ice-cold PBS and lysed in 2 pellet volumes of Buffer C (300 mM NaCl, 20 mM HEPES pH 7.9, 20% glycerol, 2 mM MgCl2, 0.2 mM EDTA, 0.1% NP-40, 1x cOmplete Protease Inhibitor Cocktail (Sigma-Aldrich), 1x PhosStop™ (Sigma-Aldrich), 10 μM Olaparib (Selleckchem), 2 mM NEM (Sigma-Aldrich) and 0.5 mM DTT) by

incubation for 90 min in a rotation wheel at 4°C. After centrifugation (2000 g, 30 min, 4°C), the soluble nuclear extract was collected, the concentration of EDTA was adjusted to 2 mM and the extract was snap frozen.

Chromatin-enriched nuclear extracts were prepared by using a modified protocol for nuclear extraction. Briefly, nuclear extracts were first generated, after which the remaining insoluble chromatin pellet was resuspended in 4 pellet volumes of RIPA buffer (150 mM NaCl, 50 mM Tris pH 8.0, 1% NP-40, 5 mM $MgCl_2$, 10% glycerol, 1x cOmplete Protease Inhibitor Cocktail (Sigma-Aldrich), 1x PhosStop™ (Sigma-Aldrich), 10 μM Olaparib (Selleckchem) and 2 mM NEM (Sigma-Aldrich)) supplemented with 1,000 U benzonase nuclease (Sigma-Aldrich) per 100 μL pellet. The resuspended chromatin fraction was then incubated at 37°C with vigorous shaking (1,000 rpm) until chromatin dissolved and then centrifuged (12000 rpm, 10 min, 4°C). The supernatant was collected, supplemented with EDTA (2 mM final concentration) and combined with the nuclear extract. Chromatin-enriched nuclear extract was then aliquoted and snap-frozen in liquid nitrogen until further usage.

Cells used for western blotting were washed twice in ice-cold PBS and lysed in denaturing buffer (20 mM Tris–HCl, pH 7.5; 50 mM NaCl, 1.5 mM $MgCl_2$, 0.5% NP-40, 0.5% SDS, 0.5% sodium deoxycholate, 1x cOmplete Protease Inhibitors, 1x PhosStop, 10 μM Olaparib, 5 μM PDD00017273 (PARGi), 2 mM NEM and 1 mM DTT) supplemented with benzonase nuclease (Sigma-Aldrich) (Kliza et al., 2017). The lysate was incubated for 30 min in a rotation wheel at 4°C, followed by centrifugation (13000 rpm, 20 min, 4°C). The supernatant was collected and supplemented with 10% (v/v) glycerol and EDTA to 2 mM final concentration. The extract was either used immediately or snap-frozen in liquid nitrogen and stored in −80°C until further use.

The protein concentration of lysates was measured using the Pierce BCA Protein Assay Kit (Thermo Fisher Scientific).

ADPr affinity purifications

For ADPr affinity purifications using whole-cell extracts, each ADPr probe (biotinylated mono-, di- and tri-ADPr) was individually immobilized on pre-washed Streptavidin Sepharose beads (GE healthcare Life Sciences) in 700 μL of binding buffer (50 mM Tris-HCl pH 8.0, 150 mM NaCl, 2 mM EDTA, 0.5% (v/v) NP-40, 1x cOmplete Protease Inhibitor Cocktail, 1x PhosStop™, 10 μM Olaparib, 5 μM PDD00017273 (PARGi, Tocris), 2 mM NEM and 0.5 mM DTT) for 30 min at 4°C in a rotation wheel. For label-free quantification purposes, each sample was prepared in technical triplicate. 5 nmol of each ADPr probe and 20 μL of Streptavidin Sepharose slurry were used for each affinity purification. Next, beads were washed thrice with 700 μL binding buffer, followed by incubation with 3mg of whole-cell extract in a total volume of 1 mL binding buffer on a rotation wheel for 90 min at 4°C. Samples were vigorously washed five times with 1 mL of binding buffer (1% NP-40), follow by one wash with 1 mL of binding buffer (0.5% NP-40) and three washes with 1 mL of 1xPBS. All steps were done on ice or at 4°C. Bound proteins were subjected to on-bead trypsin digestion as described in the On-bead digestion section.

ADPr affinity purifications with nuclear lysates were conducted essentially as described for whole cell lysates with several adjustments. 0.8 mg of nuclear extract was used per each replicate. Nuclear extract has higher concentration of sodium chloride (~300 mM) compared to whole cell extract. Therefore, a modified binding buffer was combined with nuclear extract to obtain a 150 mM NaCl final concentration. For DNA damage-dependent ADPr affinity purifications, similar adjustments were made to the protocol and 1.25mg of chromatin enriched extract was used for each replicate affinity purification. Each of these samples were prepared in duplicate and each of these duplicates was measured twice.

For comparisons between ADPr and biotin-triA and -pentadecaA, RNasin, inhibitor of Ribonucleases (Promega, Cat# N2111), was added to the binding buffer.

For ADPr affinity purification followed by western blotting, samples were prepared as described above, but the concentration of the ADPr probes, input protein amounts and total sample volume were scaled down by factor of 3.

To test the enzymatic stability of the biotin-ADPr probes, the ADPr affinity purification was done as described above, with following adjustments: a reference sample was prepared using buffers containing 2 mM EDTA and 5 μM PDD00017273 (PARGi), whereas remaining samples were not exposed to inhibitors of ADPr hydrolases. After the streptavidin pull-down, all samples were washed as usual, followed by three washes with PBS and two washes with cleavage buffer (50 mM Tris pH 8.0, 50 mM NaCl, 15 mM MgCl2, 0.2 mM DTT). Next, samples were resuspended in 50 ul of cleavage buffer. Designed samples were treated with either 4 μM of recombinant ENPP1 (R&D Systems) or 25 pmol of recombinant PARG (Enzo Life Sciences) for 30 min with vigorous shaking. Next, samples were washed once in cleavage buffer, followed by one wash in PBS. Proteins were eluted from streptavidin resin by incubation in a LDS buffer supplemented with β-mercaptoethanol (10 min, 70°C).

ADPr competition binding assay

The samples for ADPr competition binding assay were prepared as described in the ADPr affinity purifications section with adjustment that the incubation of pre-bound biotinylated ADPr probes (2 nmol of either biotin-monoADPr or biotin-triADPr per sample) with nuclear extracts (0.4 mg per sample) was done in the presence of various, increasing amounts of either untagged mono- or triADPr: 0, 1 and 2 nmol.

ADPr PAQMAN experiments

The ADPr PAQMAN protocol was developed by adapting the original PAQMAN method (Gräwe et al., 2020). A duplicate series of three-fold dilutions of monoADPr and triADPr probes were prepared. The lowest and highest concentration for each ADPr probe was 0.61 nM and 12 μM, respectively and 10 concentrations in total were used. Probes were diluted in ADPr-binding buffer

(50 mM Tris-HCl pH 8.0, 150 mM NaCl, 2 mM EDTA, 0.05% (v/v) NP-40, 1x cOmplete Protease Inhibitor Cocktail and 5 μM PDD00017273 (PARGi). 96-well filter plates (Millipore, Cat#MSBVS1210) were washed with 70% ethanol (v/v), followed by two washes with ADPr-binding buffer. Sixteen microliters of Streptavidin Sepharose slurry were added to each well and washed twice with ADPr-binding buffer. A series of diluted ADPr probes were then added separately to individual filter plate wells. Probes were immobilized on the Streptavidin Sepharose beads for 1 h at 4°C. For efficient immobilization, the filter plate was placed on a tabletop microplate shaker at 85 rpm. Next, ADPr probes pre-bound to the beads were washed once with ADPr-binding buffer, followed by two washes with ADPr:Protein incubation buffer (50 mM Tris-HCl pH 8.0, 150 mM NaCl, 2 mM EDTA, 0.25% (v/v) NP-40, 1 mM Tris(2-carboxyethyl)phosphine (TCEP, Sigma-Aldrich), 1x cOmplete Protease Inhibitor Cocktail and 5 μM PDD00017273 (PARGi)). Per well, 100 μg of Olaparib-treated HeLa nuclear extract was diluted in modified ADPr:Protein incubation buffer to reach 150 mM final concentration of NaCl. Diluted protein extract was added to each well and samples were incubated shaking for 2 h at 4°C. Next, samples were washed six times with buffer containing 100 mM triethylammonium bicarbonate (TEAB) and 150 mM NaCl.

Bound proteins were eluted by incubation with elution buffer (80 mM TEAB, 20% methanol (v/v), 10 mM TCEP) for 30 min at RT with agitation. Iodoacetamide (Sigma-Aldrich) was added to each sample for protein alkylation, followed by overnight trypsin digestion at RT. Samples were then labeled with 10-plex TMT (Thermo Fisher Scientific). Ten microliters of TMT reagent diluted in anhydrous acetonitrile was mixed with each corresponding sample and incubated for 1 h in the dark, with agitation. Reactions were quenched with 100 mM Tris, pH 8.0 for 30 min at RT, after which samples were combined. Samples were acidified with 10% (v/v) trifluoroacetic acid, and desalted using StageTipping (Rappsilber et al., 2007).

On-bead digestion

On-bead trypsin digestion was performed as described previously (Spruijt et al., 2013). Briefly, the remaining supernatant was removed from the beads, followed by elution with buffer containing 2 M urea, 50 mM Tris pH, 8.5 and 10 mM DTT (20 min, RT, 1200 rpm). Alkylating agent iodoacetamide (Sigma-Aldrich) was added to sample at 55 mM final concentration and incubated in the dark (10 min, RT, 1200 rpm). Next, sample was incubated with 250 ng of trypsin (2 h, RT, 1200 rpm), followed by centrifugation (2 min, RT, 4000 rpm) and supernatant collection. A second round of protein elution was performed (10 min, RT, 1200 rpm). After centrifugation, both eluates were combined and an additional 200 ng of trypsin was added. The protein digestion was performed overnight at RT. Next day, trypsin activity was inhibited by sample acidification to pH < 2 with 10% (v/v) trifluoroacetic acid followed by peptide desalting using the StageTip method.

Chemical synthesis of biotinylated oligoADPr probes

The detailed description of the chemical synthetic route and quality checks of prepared ADPr probes is enclosed in Methods S1.

ADPr affinity purification with recombinant proteins

The experiment was performed for the following recombinant proteins: MKRN2-GST (Abnova), MECP2-GST (Abnova), THOC6/WDR58-GST (Abnova), XRCC1-GST (Abnova), IMPDH-HIS (Origine) and negative control GST-HIS (Mybiosource). Three microliters of Streptavidin Dynabeads MyOne C1 beads were washed three times with 1 ml of PBS, followed by incubation with 0.5 μg/μl BSA diluted in PBS (overnight, 4°C, agitation). Next day, beads were washed thrice with 1 mL of PBS and then resuspended in the buffer containing 50 mM Tris-HCl, pH 8.0, 150 mM NaCl, 1 mM EDTA, 0.1% (v/v) NP-40, 1x cOmplete Protease Inhibitor Coctail and 5 μM PDD00017273 (PARGi). Next, ADPr probes (100 pmol) diluted in the same buffer were incubated with the beads for 30 min at 4°C, rotating. After incubation, the bait-bound beads were washed thrice with the buffer, followed by resuspension in the incubation buffer (50 mM Tris-HCl pH 8.0, 150 mM NaCl, 1 mM EDTA, 0.5% (v/v) NP-40, 5% glycerol, 1x cOmplete Protease Inhibitor Coctail and 5 μM PDD00017273 (Olaparib)). Recombinant GST- or HIS-tagged proteins (~5-20 pmol) were then added to the beads and incubated for 1.5 h at 4°C, rotating. Next, samples were washed four times with 1 mL of the incubation buffer containing 1% NP-40 (v/v), one time with 1 mL of the incubation buffer containing 0.5% NP-40 (v/v) and once with 1 mL of PBS. The supernatant was removed completely, beads were resuspended in 5x SDS loading buffer supplemented with β-mercaptoethanol and bound proteins were eluted at 70°C for 10 min.

In vitro ubiquitination assay

Recombinant 200 ng UBE1 (E1, BostonBiochem), 200 ng UbcH5a/UBE2D1 (E2, BostonBiochem), 300 ng MKRN2-GST (Abnova) and 200 ng Ub (BostonBiochem) were diluted in *in vitro* ubiquitination buffer (25 mM Tris, pH 7.5, 100 mM NaCl, 5 mM $MgCl_2$, 1.5 mM DTT, supplemented with $MgCl_2$-ATP (BostonBiochem)). In sample 1 (lane 1 in Figure 3I) MKRN2-GST was omitted. $MgCl_2$-ATP was absent in sample 2 (lane 2 in Figure 3I). Prior to the *in vitro* ubiquitination assay, MKRN2-GST was pre-incubated for 30 min at 4°C with either 0.25 μM of biotinylated PAR polymers (Trevigen) or corresponding volume of the buffer, in which PAR was diluted. Samples 4 and 6 (lanes 4 and 6 in Figures 3I) contain PAR chains. The final volume of the reactions was 25 μl. The *in vitro* ubiquitination incubation time for each sample is indicated in the figure.

Immunoblotting

Immunoblotting was performed as described previously (Kliza et al., 2017). Briefly, proteins were separated by SDS–PAGE and transferred to 0.22 μm nitrocellulose membrane by wet transfer at 200 mA for 2 h. Membranes were blocked in 5% non-fat dried milk in

TBS-T and probed with indicated primary antibodies for either 1 h at RT or overnight at 4°C. Next, membranes were thrice washed in TBS-T, incubated in an appropriate HRP-conjugated secondary antibody for 1 h at RT and washed three times in TBS-T and then once in TBS. Membranes were developed using Pierce ECL Western Blotting Substrate (Thermo Fisher Scientific) and analyzed by ImageQuant™ LAS-4000 (GE Healthcare). Following antibodies were used for immunoblotting: mouse monoclonal XRCC1 (Cat#sc-56254), mouse monoclonal ATR (Cat#sc-515173), mouse monoclonal DLD (Cat#sc-365977), rabbit monoclonal GAPDH (Cat#2118S), mouse monoclonal IMPDH (Cat#sc-166551), mouse monoclonal KIF14 (Cat#sc-365553), mouse monoclonal ME2 (Cat#sc-514850), mouse monoclonal MKRN2 (Cat#sc-514185), rabbit polyclonal MKRN2 (Cat#ab72055), mouse monoclonal MVP/LRP (Cat#sc-23916), mouse monoclonal NOLC1/NOPP140 (Cat#sc-374033), mouse monoclonal SFPQ/PSF (Cat#sc-374502), mouse monoclonal TDP1 (Cat#sc-365674), mouse monoclonal THOC1 (Cat#sc-514123), mouse monoclonal THOC5/FMIP (Cat#sc-514146), mouse monoclonal THOC6 (Cat#sc-390722), rabbit polyclonal ZC3H14 (Cat#orb422692), rabbit polyclonal MACROD1 (Cat#NBP2-85248), rabbit polyclonal OGFR (Cat#NBP2-83799), mouse monoclonal TUBA1A (Cat#T5168), mouse monoclonal GST (Cat#sc-138), rabbit polyclonal HIS (Cat#CST 2365T), mouse monoclonal Ub (P4D1) (Cat#Sc-8017), rabbit polyclonal Streptavidin-HRP conjugated (Cat#PA1-26848), rabbit monoclonal H2AX (Cat#7631S), rabbit monoclonal γH2AX (Cat#9718S), rabbit polyclonal GFP (Cat#ab290).

The results of immunoblotting in Figures 3F, 3G, and 3I were quantified using ImageJ/Fiji and were normalized using indicated controls. Results of quantification of Figures 3F and 3G are presented in tables in Figures S3F and S3G, respectively. Quantification of Figure 3I is illustrated by a plot in Figure 3J.

Proteome analysis

The proteome of HeLa and HaCaT cells was determined using following protocol: proteins were concentrated by aceton precipitation, followed by denaturation in the buffer containing 8 M urea, 0.1 M Tris pH 8.5 and 10 mM DTT. Next, FASP protocol (filter aided sample preparation method) was used to digest the proteins using trypsin (Wiśniewski et al., 2009).

Mass spectrometry

The samples were loaded onto a column (30 cm length, 75 μm inner diameter) in-house packed with Reprosil-Pur C18-AQ beads (Dr. Maisch). Tryptic peptides were eluted from a reverse-phase EASY-nLC connected online to either an LTQ-Orbitrap Q-Exactive, Orbitrap Exploris 480, or Orbitrap Fusion mass spectrometer. Peptides generated in MAR and PAR PAQMAN assays were separated using a buffer B gradient (80% acetonitrile, 0.1% formic acid) comprising of the following steps: 7%–15% gradient over 5 min, 15%–35% over 214 min, 35%–50% over 5 min, 50%–95% over 1 min, followed by 95% buffer B over 5 min (flow rate 200 nl/min). Total data acquisition time was 240 min. The processed HeLa and HaCaT proteome samples were measured using an initial 43-min gradient of buffer B (12%–30%), followed by gradient increase up to 60% over 10 min and further up to 95% over 1 min (flow rate 200 nl/min). Total data-collection time was 60 min. For remaining proteomics experiments, peptides were separated using a 114-min gradient of buffer B (7%–32%), followed by a segmented increase up to 95% buffer B (flow rate 200 nl/min). Total data acquisition time was 140 min.

All scans were collected with a top20 acquisition mode enabled and mass spectra were recorded.

QUANTIFICATION AND STATISTICAL ANALYSIS

General information

Information on quantifications for each method is provided in the respective Method details section. The number of independent replicates for each immunoblotting-based experiment is provided in the figure legend. Details of statistical analyses are provided in the Results section and in the figure legends. Data in Figures 2B and S3A are represented as mean ± SEM and *$p < 0.05$, **$p < 0.01$, ***$p < 0.005$.

Mass spectrometry data analysis

Raw data was analyzed using MaxQuant version 1.5.0.1 with default settings and searched against the UniProt human proteome (year of release: 2017) (Cox and Mann, 2008). Additionally, match between runs, label-free quantification and IBAQ quantifications were enabled. Common contaminants, reverse hits and proteins identified only by site were filtered out. LFQ intensities were $\log_2$ transformed and additional filtering was applied to detect proteins present in all replicates of at least one experimental triplicate. Missing values were imputed from a normal distribution (width = 0.3 and shift = 1.8) in Perseus (version 1.5.0.15), assuming that these proteins were just below the detection limit (Tyanova et al., 2016). For data visualization in Volcano plots, two sample t test analysis was performed (FDR ≤ 0.05, FC ≥ 2, for each experiment specified in the text). For data representation as heatmaps or radar charts, protein enrichments were normalized by Z-score calculations prior to an ANOVA test (thresholds are indicated in the Results section for each specific experiment). The hierarchical clustering of significantly enriched proteins was performed (Euclidean distance, complete linkages). The data visualization, which includes Volcano plots, heatmaps, regular and circular boxplots, correlation, dot and Cleveland plots, radar charts and Venn diagram, were done in R. Data correlation in Figure 6B, was done using ComplexHeatmap package in R (Gu et al., 2016).

PAQMAN experiments were analyzed as shown in detail elsewhere (Gräwe et al., 2020). TMT-based quantification, spectral matching to peptides, peptide identification grouping into proteins, and isobaric label quantification were performed using Proteome Discoverer 2.2 (Thermo Scientific). The pre-defined processing workflow "PWF_Fusion_Reporter_Based_Quan_SPS_MS3_SequestHT_Percolator" and the consensus workflow "CWF_Comprehensive_Enhanced Annotation_Quan_Results" were used. The TMT 10-plex quantification method was enabled with the 131 mass set as the control channel. Initial data exploration revealed that in all replicates one condition (128C) showed significant deviation, therefore this channel was disabled from quantification. For the Sequest HT search, database parameters were set to: tryptic digestion allowing two missed cleavages, peptide length between 6 and 144 amino acids. The search was performed against the UniProt human proteome. A precursor mass tolerance of 10 ppm and a fragment mass tolerance of 0.6 Da were used. The following modifications were included: cysteine carbamidomethylation (57.021 Da, static modification), methionine oxidation (15.995 Da, dynamic modification) and protein N-terminal acetylation (42.011 Da, dynamic modification). Moreover, the 6-plex TMT reagent mass (229.163 Da) was included as a dynamic modification enabled on lysine, histidine, serine, and threonine residues, as well as the N terminus of the peptide. A strict target FDR of 0.01 and a relaxed FDR of 0.0532 were set up for FDR filtering. Strict parsimony was applied for protein grouping, and only unique peptides were used for quantification. No peptide quantification normalization was applied. The calculation of protein binding parameters, fitting Hill-like curve ($R^2 \geq 0.90$) for each identified protein and plot generation was done as described previously, using in-house Python script. The heatmaps for PAQMAN experiment were done in R.

The GO enrichment analysis was performed using DAVID 6.8 (Huang et al., 2009a, 2009b). All proteins detected in the experiment were used as background against significant interactors. The statistically significantly enriched terms were identified using default settings in DAVID. The results were visualized as dot plots in R.

To determine putative ADPr-binding domains of identifiedMS candidates, a search in ScanProSITE and InterPro was performed (de Castro et al., 2006; Blum et al., 2021). The database of proteins identified as significant interactors in experiments from Figures 1, 2, 3, and 4 was generated and protein sequences of identified ADPr readers were screened for presence of consensus PAR-binding sequences (one PAR-binding module search at a time) (Kamaletdinova et al., 2019). Scanning at high sensitivity was enabled, match mode greedy, includes, overlaps was chosen. The predicted putative PAR-binding domains with the low scores were not taken under consideration and are not present in the Figures 5C and S5B. The results of the analysis were summarized in dot plots made in R and Table S1. An exemplary alignment visualization was performed in Jalview editor (Waterhouse et al., 2009). The ADPr interactors: disease relations were done by mining the OMIM and DisGeNET databases and summary of this analysis is presented in Table S1 (Amberger et al., 2009; Piñero et al., 2019).